IOP Publishing Phys. Med. Biol. 66 (2021) 10TR03 https://doi.org/10.1088/1361-6560/abf276

Physics in Medicine & Biology

IPEM Institute of Physics and Engineering in Medicine

OPEN ACCESS

RECEIVED
9 December 2020

REVISED
3 March 2021

ACCEPTED FOR PUBLICATION
26 March 2021

PUBLISHED
14 May 2021

TOPICAL REVIEW

Advanced Monte Carlo simulations of emission tomography imaging systems with GATE

David Sarrut[1,*], Mateusz Bała[2], Manuel Bardiès[3], Julien Bert[4], Maxime Chauvin[5], Konstantinos Chatzipapas[6], Mathieu Dupont[7], Ane Etxebeste[1], Louise M Fanchon[8], Sébastien Jan[9], Gunjan Kayal[5,10], Assen S Kirov[8], Paweł Kowalski[11], Wojciech Krzemien[11], Joey Labour[1], Mirjam Lenz[12,13], George Loudos[6], Brahim Mehadji[7], Laurent Ménard[14,15], Christian Morel[7], Panagiotis Papadimitroulas[6], Magdalena Rafecas[16], Julien Salvadori[17], Daniel Seiter[18], Mariele Stockhoff[19], Etienne Testa[20], Carlotta Trigila[21], Uwe Pietrzyk[13], Stefaan Vandenberghe[19], Marc-Antoine Verdier[14,15], Dimitris Visvikis[4], Karl Ziemons[12], Milan Zvolský[16] and Emilie Roncali[21]

[1] Université de Lyon, CREATIS, CNRS UMR5220, Inserm U1294, INSA-Lyon, Université Lyon 1, Lyon, France
[2] Jagiellonian University, Kraków, Poland
[3] Cancer Research Institute of Montpellier, U1194 INSERM/ICM/Montpellier University, 208 Av des Apothicaires, F-34298 Montpellier cedex 5, France
[4] LaTIM, INSERM UMR 1101, IBRBS, Faculty of Medicine, Univ Brest, 22 avenue Camille Desmoulins, F-29238, Brest, France
[5] CRCT, UMR 1037, INSERM, Université Toulouse III Paul Sabatier, Toulouse, France
[6] Bioemission Technology Solutions (BIOEMTECH), Alexandras Av. 116, Athens, Greece
[7] Aix-Marseille Univ, CNRS/IN2P3, CPPM, Marseille, France
[8] Department of Medical Physics, Memorial Sloan Kettering Cancer Center, New York, NY, 10065, United States of America
[9] Université Paris-Saclay, CEA, CNRS, Inserm, BioMaps, Service Hospitalier Frédéric Joliot, F-91401, Orsay, France
[10] SCK CEN, Belgian Nuclear Research Centre, Boeretang 200, Mol 2400, Belgium
[11] High Energy Physics Division, National Centre for Nuclear Research, Otwock-Świerk, Poland
[12] FH Aachen University of Applied Sciences, Forschungszentrum Jülich, Jülich, Germany
[13] Faculty of Mathematics and Natural Sciences, University of Wuppertal, Wuppertal, Germany
[14] Université Paris-Saclay, CNRS/IN2P3, IJCLab, F-91405 Orsay, France
[15] Université de Paris, IJCLab, F-91405 Orsay France
[16] Institute of Medical Engineering, University of Lübeck, Lübeck, Germany
[17] Department of Nuclear Medicine and Nancyclotep molecular imaging platform, CHRU-Nancy, Université de Lorraine, F-54000, Nancy, France
[18] Department of Medical Physics, University of Wisconsin-Madison School of Medicine and Public Health, Madison, WI, 53705, United States of America
[19] Medical Image and Signal Processing (MEDISIP), Ghent University, Ghent, Belgium
[20] Univ. Lyon, Univ. Claude Bernard Lyon 1, CNRS/IN2P3, IP2I Lyon, F-69622, Villeurbanne, France
[21] Department of Biomedical Engineering, University of California, Davis, CA 95616 United States of America
[*] Author to whom any correspondence should be addressed.

E-mail: david.sarrut@creatis.insa-lyon.fr

Keywords: Monte Carlo simulation, Positron emission tomography, Single-photon emission computed tomography, Compton Camera

Abstract

Built on top of the Geant4 toolkit, GATE is collaboratively developed for more than 15 years to design Monte Carlo simulations of nuclear-based imaging systems. It is, in particular, used by researchers and industrials to design, optimize, understand and create innovative emission tomography systems. In this paper, we reviewed the recent developments that have been proposed to simulate modern detectors and provide a comprehensive report on imaging systems that have been simulated and evaluated in GATE. Additionally, some methodological developments that are not specific for imaging but that can improve detector modeling and provide computation time gains, such as Variance Reduction Techniques and Artificial Intelligence integration, are described and discussed.

1. Introduction

GATE is an open-source, community-based software effort relying on the Geant4 toolkit (Allison *et al* 2016) dedicated to Monte Carlo simulation in medical physics. GATE is about 15 years old and evolves a lot through

users' contributions. It was initially focused on nuclear imaging (Santin *et al* 2003, Strul *et al* 2003, Jan *et al* 2004, Buvat and Lazaro 2006), then expanded to external and internal radiotherapy (Jan *et al* 2011), dosimetry (Sarrut *et al* 2014) and hadrontherapy (Grevillot *et al* 2020). The simulated physics is managed by the Geant4 Monte Carlo kernel in charge of tracking particles in matter and processing physical interactions. On top of Geant4, GATE gathers multiple developments that facilitate medical physics simulations. Indeed, numerous clinical, preclinical, and prototype positron emission tomography (PET) and single photon emission compute tomography scanners were simulated and confronted with experimental data.

Since the initial 2004 OpenGATE collaboration article, emission tomography systems have changed dramatically (Vandenberghe *et al* 2020) with improved time-of-flight (TOF) methods, better detection systems based on silicon photomultipliers (SiPMs), long axial field of views (FOVs), multi-headed systems, etc. At the same time, Monte Carlo simulation also had to evolve to support those developments. This type of simulation remains the gold standard for design, optimization and assessment of imaging systems, and serves to estimate their performance, to optimize acquisition parameters, and to design reconstruction algorithms.

Since then, no synthesis of emission tomography (SPECT, PET, Compton Camera) capabilities of GATE has been published. The goal of this paper is to review the current GATE capabilities and limitations for simulating emission tomography imaging systems. The article is organized in the following way: section 2 describes the recent developments for detector simulations, section 3 gives more details about validated simulated imaging systems, and finally section 4 reports on additional developments not specific to emission tomography yet helpful to the field.

2. Detector developments

In the following, we describe the main modules recently developed or updated for simulation of modern emission tomography systems. The first subsection summarizes the two main modes of simulation, then, we describe optical photon tracking, Cerenkov-based TOF and Compton camera modules (CCMod).

2.1. Principal simulation modes

In nuclear imaging, events are usually detected by collecting scintillation photons emitted after energy deposition of high-energy gamma photons in inorganic crystals (LYSO[22], LSO[23], BGO[24], etc) using photodetectors such as photomultiplier tubes (PMT), avalanche photodiodes (APDs) or SiPMs (Roncali and Cherry 2011). There are two modes that can be used in GATE to simulate this detection stage.

The first mode consists in full Monte Carlo tracking of the emitted optical photons. In such simulations, precise definition of the crystal optical surfaces is crucial to obtain a realistic light distribution. While it is useful to design and to better understand the in-depth behavior of a given detection system, simulating all optical photons leads to long computation times due to the very large number of tracked particles (Cherry *et al* 2012). This first mode will be presented in section 2.2.

In the second simulation mode in GATE, the response of the photodetection components is simulated by a specific module called a *digitizer*. In that case, an analytical model is used to generate detection events from the list of interaction events within the crystal, assuming the number of generated digital pulses is proportional to the number of scintillation photons in the crystal. This *digitizer* converts photon interactions in the crystal into digital counts and assigns time stamps to every event. Numerous parameters are provided to the user who can apply successive signal processing operations to generate a final response adapted to the hardware: pixelated or monolithic scintillator detectors, depth-of-interaction (DoI) modeling, dead time, etc. Moreover, various stochastic uncertainties can be added to reproduce the intrinsic resolution of components such as the intrinsic radioactivity of ^{176}Lu in LSO (McIntosh *et al* 2011), or the intrinsic resolution of a particular scintillator (Jan *et al* 2004).

A specific vocabulary is used: *hits*, *singles*, *coincidences*. Individual particle interactions within a detector element (e.g. crystal) are called *hits*, each *hit* containing information about the interaction process type, the position, deposited energy, time, the volume where the interaction occurs, etc. The *hits* within the same readout volume are gathered into *singles. Singles* are sorted by time-stamp and associated in *coincidences* according to several rules, in particular to handle coincidence windows during which more than two singles are detected. In PET imaging, it is common to consider several types of coincidences: the *scatters* (coincidence events resulting from scattered photons inside the subject), the *randoms* (accidental coincidences), the *trues* (real, expected coincidences). The sum of those three types are called the *prompts* (total detected coincidences). In reality, the

[22] Lutetium–yttrium oxyorthosilicate.

[23] Lutetium oxyorthosilicate.

[24] Bismuth germanium oxide.

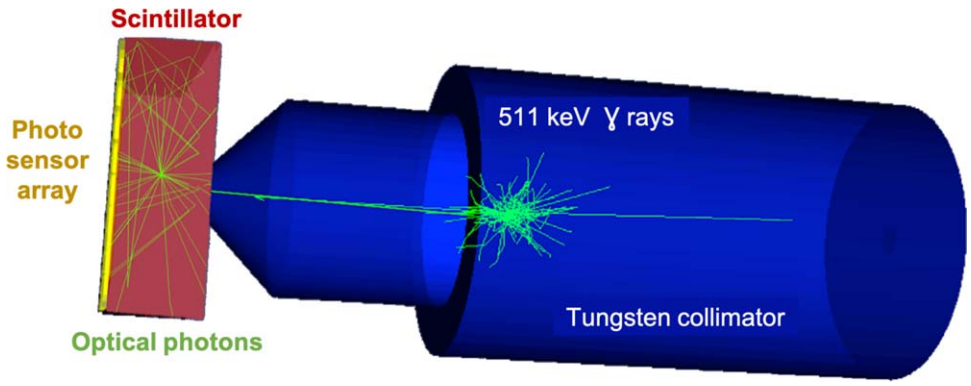

Figure 1. Optical simulations of a calibration setup for monolithic scintillators. A $50 \times 50 \times 16\,mm^3$ LYSO crystal was modeled read out by a pixelated array of photo-detectors. The scintillator surfaces are defined by the LUT Davis reflection model based on measured data. The calibration beam is encapsulated in a tungsten collimator which is simulated by importing the 3D STL file into GATE. The source is a monoenergetic 511 keV gamma point source.

number of *randoms* is not known from experimental data and is estimated by the *delay* coincidences obtained from delayed time coincidence windows (Strydhorst and Buvat 2016a). GATE generates all types of coincidences for detailed analysis.

The digitizers processes are common to PET, SPECT and CCMods and may be used either 'online', during the Monte Carlo particle tracking, or 'offline', after the end of the simulation. In this latter case, the simulation output requires *hits*, *singles*, and/or *coincidences* data to be saved in root (or Python) files that can be post-processed. More details can be found in Strydhorst and Buvat (2016a), Etxebeste *et al* (2020).

2.2. Optical photon tracking and SiPM

The precise definition of crystal optical surfaces can be modeled with the *Davis look-up table (LUT) surface reflection model*, introduced in GATE since version 8.0 (Stockhoff 2017). This model is based on measured surface data obtained by atomic force microscopy. Users can choose between two surfaces, a polished and a rough one. For each surface, four LUTs are available: LSO crystal with no reflector, coupled to Teflon through an air interface, ESR-air and ESR-grease. The models consider optical photon reflection probabilities and directions depending on the incidence angle of the photon on the crystal surface. The models were validated against experimental data. Next step towards finer detector modeling lies in the use of completely customized LUTs. For this reason, a standalone user interface has been developed to allow users to generate LUTs for any surface obtained with a 3D scanning method with a sub-micron resolution with the personalized definition of the intrinsic properties of the scintillator and the coupling medium and a specific reflector attached to the crystal, Trigila *et al* (2021). The LUTDavis model has been validated for several configurations by comparing the experimental and simulated light output of single crystals, with an error of less than 10% (Roncali and Cherry 2013).

With the *LUTDavis model*, a large monolithic scintillation detector for clinical PET systems was simulated using optical photon tracking. The detector consisted of $50 \times 50 \times 16\,mm^3$ LYSO coupled with optical grease to an array of SiPMs (see figure 1). The gamma entrance face was defined with the polished ESR LUT. The crystal sides were defined with an adapted LUT modeling a rough surface with black paint leading to absorption of photons transmitted by the crystal surface. The SiPM readout side was simulated by LUTs that model polished surfaces and take into account the index of refraction of optical grease. Optical simulations were used to optimize the performance of the detector by testing various setups and their influence on the desired performance parameter. It was thus possible to gain insight into physical processes that are difficult or impossible to measure experimentally, notably ground-truth interaction positions, especially DoI. Each influencing factor can be analyzed separately as for example the influence of Compton scattered events, the influence of intrinsic ^{176}Lu radiation of the scintillator, the influence of test-equipment, e.g. collimators or housing.

In Stockhoff *et al* (2019), the focus was set on the spatial resolution influenced by the size of the photodetector pixels, the photon detection efficiency (PDE) and the number of channels used to read out the sensor array. The outcome of this simulation study demonstrated the high spatial resolution of 0.4–0.66 mm full width at half maximum (FWHM) that can be obtained by a monolithic detector under idealized configurations. High PDE and small pixel sizes improved the resolution, while the number of electronic readout channels could be decreased drastically by summing rows and columns with only a small or no degradation on the spatial resolution. In Decuyper *et al* (2019, 2021) the performance of the detector could further be improved by using

artificial neural networks (ANNs) to train the positioning algorithm. The simulation was used to identify and address potential pitfalls related to ANNs which could then be translated to the experimental results. @Mariele do you have any validation numbers to add? The simulation of single detector modules does not only require a dedicated surface modeling, but also has to account for the detection of scintillation photons and the subsequent pulse processing inside the photodetector. The increasing use of SiPMs (see section 2) in the context of PET imaging (Lewellen 2008, Cabello and Ziegler 2018, Conti and Bendriem 2019) motivated the implementation of specific *digitizer modules* for analog and digital SiPMs (dSiPMs), so that both the complete scanner system and the single detector modules can be simulated.

First, a digitizer module for *analog SiPMs (aSiPMs)* was implemented, allowing to reproduce signals originating from aSiPMs. For each optical photon impinging onto the surface of detection, a pulse has a non-null probability to be generated at a time $t + \Delta t$ considering the PDE, where t corresponds to the time of the detection and Δt accounts for the single photon time resolution. The digitizer also takes into account aSiPM saturation and various sources of noise such as dark counts, crosstalks, afterpulses, after-crosstalks and signal white noise (Mehadji 2020).

A second digitizer module was implemented for *dSiPMs*, referring to the Philips digital photon counter (DPC). A DPC sensor tile is subdivided into 16 so-called dies, which comprise four pixels each and are read out independently. In contrast to aSiPMs, this device stores the number of counted photons on the four pixels of a die and a die timestamp for each event. It therefore delivers a completely digital signal. Furthermore, it makes use of a trigger and validation logic in order to reduce the recording of dark counts (Degenhardt *et al* 2009, Frach *et al* 2009). This dedicated digitizer currently allows for consideration of the most relevant noise sources (dark noise and optical crosstalk), the PDE of the sensor, and the specific trigger and validation logic. For validation of the model, the probabilities for trigger and validation, determined by Tabacchini *et al* (2014), have been successfully reproduced (Lenz 2020).

2.3. Cerenkov-based TOF

The use of ultra-fast (10 ps) Cerenkov emission for TOF PET detectors has been investigated extensively as an alternative to traditional time triggering on scintillation photons emitted within tens to hundreds of ns (Lecoq 2012, Somlai-Schweiger and Ziegler 2015, Brunner and Schaart 2017, Kwon *et al* 2016, Cates *et al* 2018). The potential of Cerenkov light has become the foundation of a paradigm shift in TOF PET, with initiatives such as the 10 ps TOF challenge (Lecoq 2017, Schaart *et al* 2020, Lecoq *et al* 2020). The very low number of Cerenkov photons produced by each gamma interaction in the Cerenkov radiator (around 15–20 per photoelectric interaction for BGO) is the main limitation in fully exploiting these photons and warrants thorough studies to better understand their production, transport, collection and conversion into an electric signal. This can only be achieved through detailed simulation, as it is not possible to separate these components experimentally.

GATE has been increasingly used to study Cerenkov emission for its ability to model all aspects of the optical detection chain including the effect of optical surfaces. However, it requires modifications to tag the Cerenkov photons in the *hits* tree and associate them to their parent gamma event (Ariño-Estrada *et al* 2020, Kwon *et al* 2019, Roncali and Kwon 2019) and does not include tools for a complete optical analysis. Studies have been reported in two materials: the well-known scintillator BGO, and the novel semi-conductors thallium bromide (TlBr) and thallium chloride (TlCl). In BGO, GATE simulations of the Cerenkov production and transport in the crystal described the direction of the initial Cerenkov photons, as well as the contribution of Cerenkov photons to the detector timing resolution. These simulation studies, in excellent agreement with experimental results, provided a new explanation of the long tails in the timing spectrum observed experimentally in BGO by several groups. GATE simulations in a dual-ended readout BGO detector also elucidated the nature of the time difference between the two crystal ends by identifying the type of photon first detected by the photodetector (Cerenkov or scintillation). In TlBr and TlCl, GATE simulations were used to generate and track Cerenkov photons from the emission point to the photodetector (Ariño-Estrada *et al* 2020). The number of photons produced and detected per photoelectric interaction was estimated from the simulations, indicating the potential of TlCl as a Cerenkov radiator thanks to its optical properties. Using the simulated photon time stamps, the timing spectrum for different trigger thresholds was computed and confirmed the advantage of TlCl. Good agreement was obtained between simulations and experiments, with an overestimation of the number of detected photons of 12% (Ariño-Estrada *et al* 2020).

2.4. Compton camera modules

The recent GATE CCMod (Etxebeste *et al* 2020) provides a framework where different Compton camera configurations can be simulated and facilitates comparison between the performance of different prototypes in medical experimental settings such as hadron therapy monitoring or nuclear medicine. CCMod is designed to reproduce the response of most common configurations in medical applications composed of a *scatterer* and an

absorber detectors working in time coincidence (Everett *et al* 1977). However, it can be adapted to accommodate other designs such as one single detector layer system that acts as scatterer and absorber at the same time (Lehner *et al* 2004, Mihailescu *et al* 2007, Maier *et al* 2018, Montémont *et al* 2017) frequently employed in homeland security applications.

In CCMod, volumes defined as detector layers act as Geant4 sensitive detectors. The detector response (the list of *singles*) is simulated by applying sequentially a chain of digitizer modules to the stored information of particle interactions. The same data structure in SPECT or PET systems is employed so that digitizer modules may be applied interchangeably to all three types of imaging devices. Since in Compton cameras different detector layers have usually different roles and characteristics, digitizer modules that can be applied independently to each detector layer have been included. *Singles* are sorted into coincidences using the sorter developed for PET systems (Strydhorst and Buvat 2016a). Additional options have been included for CCMod such as allowing only *singles* in a specific detector layer (absorber) to open its own time coincidence window. Besides, different criteria for coincidence acceptance are available such as requiring at least one single in each detector type. Since, in a Compton camera system, the order of the *singles* within each coincidence determines the estimated cone surface where the source is located, a dedicated coincidence processor has been included for coincidence sequence reconstruction. At each step of this processing, from interactions to cone information, corresponding data output is available. This recent extension of GATE (Etxebeste *et al* 2020) has been successfully validated against experimental data and employed to predict the performance of prototypes under construction (see section 3).

3. Simulation of imaging systems and applications

This section reviews the emission tomography imaging systems that were simulated and, at least partially, validated against experimental data in GATE. In addition to detector development, and since the very first version, GATE has been used to simulate complete clinical and preclinical imaging systems. Efforts have been made to provide comparison against experimental data and improve the simulation when discrepancies have been found. The tables 1 and 2 list some studies and the associated clinical and preclinical imaging systems (some are illustrated figure 2). Most systems were PET scanners and, to a lesser extend, SPECT devices. CCMod in GATE is very recent (Etxebeste *et al* 2020) and only one validation against experimental data has been reported to date. Most of the evaluation methodologies were based on NEMA protocols and compared noise equivalent count rate (NECR), sensitivity, resolution, etc between simulated and experimental data. In the following we described some more recent studies, focusing on recent developments such as the use of SiPMs or TOF.

Philips Vereos Digital PET/CT. In Salvadori (2020), a detailed model of the Vereos^{TM} DPC-PET was proposed. This PET device, introduced in 2013, is one of the first PET/CT using SiPM detectors, together with, the GE Dicovery^{TM} MI PET/CT in 2016 and the Siemens Biograph Vision^{TM} in 2018. On such systems, the location of β^{+} annihilation is improved by the use of increase TOF resolution due to the use of SiPMs (210–378 ps). Moreover, the DPC system provides 1:1 coupling between the crystal array and the SiPM array, contributing to decrease uncertainty in the interaction position and to improve the image resolution.

The GATE model of the Vereos described the hierarchical structure of all the detection modules, for a total of 23 040 LYSO scintillator crystals ($4 \times 4 \times 19\,\text{mm}^3$). The complete digitization chain was simulated including background noise (natural radioactivity of ^{176}Lu in the crystals), dead time and pile-up, temporal resolution and detector quantum efficiency. The model has been evaluated following NEMA NU 2-2018 guidelines, including NECR, scatter fraction, TOF and energy resolution, sensitivity and spatial resolution. The authors reported very good agreement between experiments and simulations for clinical activity concentrations, with differences at maximum lower than 10%, concluding that the proposed GATE model can be used to very accurately reproduce PET images from Vereos system.

PET2020 long axial FOV PET. In Abi Akl *et al* (2019), Vandenberghe *et al* (2017) a long axial FOV PET scanner was simulated in GATE. Each ring consists of 36 detector modules made up of $50 \times 50 \times 16\,\text{mm}^3$ monolithic LYSO crystals. The system has an inner diameter of 65 cm. GATE was used to study the effect and advantage of axial lengths between standard 20 cm, 1 m and 2 m long systems, covering the whole human body versus a coverage of only head-to-hip. A 104 cm long system was 16 times more sensitive than a system with 20 cm axial length (1 m long uniform phantom). The effect of axial splitting of the detector rings to increase the FOV was also studied, in turn for sensitivity as well as an adaptive system bore that allows a sensitivity gain and advantages in spatial resolution due to the reduced acolinearity effect. The study showed that for objects shorter than 1 m the sensitivity gain of a 2 m scanner is limited while the detector cost is doubled compared to the 1 m system. Axial spreading is possible (at the expense of a loss in sensitivity) and an adaptive system bore can be realized by the camera aperture principle.

Table 1. Bibliography of simulated and evaluated against experimental data PET systems. LYSO: lutetium–yttrium oxyorthosilicate, LSO: lutetium oxyorthosilicate, BGO: Bismuth germanium oxide. The second column indicates if it is clinical (C) or preclinical (PC, for small animals) systems.

Bib. ref.	C/PC	PET system
2004 Assié *et al* (2004)	PC	ECAT EXACT HR+, BGO, by CPS Innovations
2004 Lazaro *et al* (2004)	PC	IASA prototype, CsI(Tl)
2004 Bataille *et al* (2004)	C	ECAT HRRT, LSO, brain
2004 Groiselle *et al* (2004)	C	prototype, CsI(NaI), by PhotoDetection Systems
2004 Rannou *et al* (2004)	PC	prototype OPET, LSO/GSO
2005 Chung *et al* (2005)	PC	prototype LSO and LuYAP
2005 Jan *et al* (2005)	C	ECAT EXACT HR+, BGO, by CTI
2006 Karakatsanis *et al* (2006)	C	ECAT EXACT HR+ and Biograph 2, by Siemens
2006 Lamare *et al* (2006)	C	Allegro/Gemini, GSO, by Philips
2006 Visvikis *et al* (2006)	PC	prototypes, CZT
2006 Michel *et al* (2006)	C	BioGraph HiRez, LSO, by Siemens
2006 Schmidtlein *et al* (2006)	C	Advance/Discovery Light Speed, BGO, by GE
2006 Merheb *et al* (2006)	PC	Mosaic, GO, by Philips
2006 Sakellios *et al* (2006)	PC	prototype, LSO
2006 Vandenberghe (2006)	C	prototype, Univ. Penn., TOF, $LaBr_3$
2006 Vandenberghe *et al* (2006a)	C	Allegro/Gemini, GSO, by Philips
2007 Gonias *et al* (2007)	C	Biograph 6, LSO, by Siemens
2007 van der Laan *et al* (2007)	PC	prototype, LSO
2007 Bruyndonckx *et al* (2007)	C	prototype, LSO
2007 Yang *et al* (2007)	PC	eXplore Vista, LYSO/GSO, by GE
2007 Vandervoort and Camborde (2007)	PC	microPET R4, Focus 120, LSO, by Siemens
2007 Rey (2007)	PC	protoype, Lausanne ClearPET
2009 Rechka *et al* (2009)	PC	LabPET, LYSO, LGSO, by Sherbrooke
2009 Geramifar *et al* (2009)	C	Discovery DLS/DST/DSTE/DRX, BGO/LYSO, by GE
2011 McIntosh *et al* (2011)	PC	Inveon, LSO, by Siemens
2011 Geramifar *et al* (2011)	C	Discovery RX, LYSO, by GE
2012 Poon *et al* (2012)	C	Biograph mCT, LSO, by Siemens
2012 Trindade *et al* (2012)	C	Gemini TF, TruFlight Select, LYSO, by Philips
2013 Lee *et al* (2013)	PC	Inveon trimodal, LSO, by Siemens
2013 Nikolopoulos *et al* (2013)	PC	Biograph DUO, LSO, by Siemens
2013 Zagni *et al* (2013)	PC	Argus, LYSO/GSO, DOI, by Sedecal
2013 Solevi *et al* (2013)	C	prototoype AX-PET, LYSO, SiPM, brain
2015 Moraes *et al* (2015)	C	Biograph mCT, LSO, by Siemens
2015 Poon *et al* (2015)	C	Biograph mCT, LSO, by Siemens
2015 Aklan *et al* (2015)	C	Biograph mMR hybrid, LSO, by Siemens
2015 Monnier *et al* (2015)	C	Biograph mMR hybrid, LSO, by Siemens
2016 Lu *et al* (2016)	PC	Inveon, LSO, by Siemens
2016 Etxebeste *et al* (2016)	PC	prototype, LYSO
2017 Sheikhzadeh *et al* (2017)	C	NeuroPET, LYSO, SiPM, brain, by PDS
2017 Li *et al* (2017)	C	Ray-Scan 64, BGO, by ARRAYS MIC
2018 Del Guerra *et al* (2018)	C	prototype TRIMAGE, LYSO
2018 Kowalski *et al* (2018)	C	prototype J-PET, plastic
2019 Abi Akl *et al* (2019)	C	prototype PET2020, LYSO
2019 Kochebina *et al* (2019)	C	prototype CaLIPSO, TMBi
2020 Emami *et al* (2020)	C	Dual ring MAMMI breast, LYSO, by Oncovision
2020 Salvadori (2020)	C	Vereos, LYSO, SiPM, Philips

CaLIPSO brain PET. The CaLIPSO PET scanner (Kochebina *et al* 2019) is a detector concept dedicated to human brain studies aiming at providing high detection efficiency with 1 mm^3 spatial resolution and coincidence time resolution (CTR) of about 150 ps. First, the prototype uses a liquid time projection chamber (see figure 4), where an elementary cell of the PET imager is filled with trimethyl bismuth (TMBi). Electrons and Cerenkov light are produced in the TMBi by γ interactions. Then, micro-channel plate PMTs (MCP-PMT) are used to detect the Cerenkov light with an excellent time resolution (85 ps FWHM). The electrons produced during the γ interactions drift along an electric field and are collected by a pixelated detector of mm^2. Ionization drift time allows to estimate depth of interaction with 1 mm precision (Ramos *et al* 2016, Canot *et al* 2017, Yvon *et al* 2020). Due to fast Cerenkov light emission, time resolution of CTR close to 150 ps (FWHM) is expected. This makes possible to use TOF technique to improve signal to noise ratio in final images.

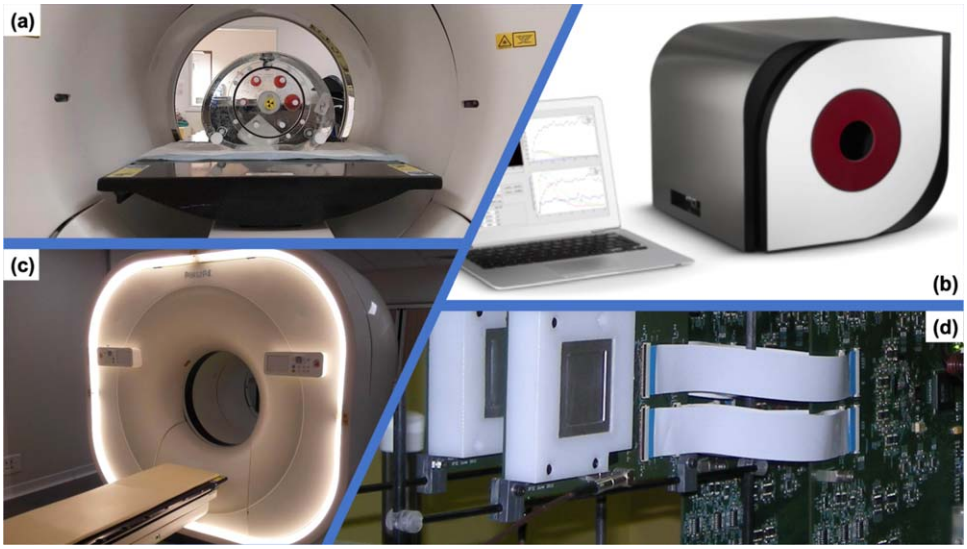

Figure 2. Examples of some simulated imaging systems (clinical, pre-clinical, prototype). (a) NEMA IEC Body Phantom Set ready to be imaged on a PET/CT. (b) The Bioemtech γ-eye preclinical device. (c) Philips Vereos Digital PET/CT; (d) MACACO Compton Camera prototype with 2 layers of $LaBr_3$ monolithic crystals coupled to SiPMs, developed by IFIC-Valencia. Reproduced with permission from Philips France Commercial.

Table 2. Bibliography of simulated and evaluated against experimental data SPECT systems. Collimators types are: low energy all purpose (LEAR), medium energy general purpose (MEGP), low energy high resolution (LEHR), high energy (HE). The second column indicates if it is clinical (C) or preclinical (PC, for small animals) systems.

Bib. ref.	C/PC	SPECT system
2003 Staelens *et al* (2003)	C	AXIS, LEHR/MEGP, ^{99m}Tc, ^{22}Na, ^{57}Co, ^{67}Ga, by Philips
2004 Assie *et al* (2004)	C	DST-Xli, MEHR, ^{111}I, by GE
2004 Assié *et al* (2004)	C	AXIS, LEHR/MEGP, ^{99m}Tc, by Philips
2004 Lazaro *et al* (2004)	PC	IASA prototype, CsI(Tl), ^{99m}Tc
2005 Staelens *et al* (2005)	C	IRIX, LEHR/MEGP, ^{99m}Tc, by Philips
2005 Autret *et al* (2005)	C	DST-XLi, Millennium VG, ^{131}I, by GE
2006 Staelens *et al* (2006)	PC	ECAM multi-pinhole, ^{123}I, by Siemens
2006 Vandenberghe *et al* (2006b)	PC	prototype SOLSITCE, solid-state, CZT, ^{99m}Tc
2006 Sakellios *et al* (2006)	PC	prototype, PSPMT, CsI(Tl), ^{99m}Tc
2008 Carlier *et al* (2008)	C	Symbia, ^{99m}Tc, ^{111}I, ^{131}I, by Siemens
2009 Park *et al* (2009)	PC	TRIAD XLT9, LEUHR, NaI(Tl), ^{99m}Tc, by Trionix
2010 Mok (2010)	PC	XSPECT, multi-pinhole, ^{99m}Tc, by Gamma Medica-Ideas
2011 Robert *et al* (2011)	C	prototype, HiSens, CZT, LEHR/H13, ^{99m}Tc, ^{57}Co
2011 Boisson *et al* (2011)	PC	prototype, parallel slat, YAP:Ce, ^{99m}Tc, ^{57}Co
2015 Lee *et al* (2015b)	PC	Symbia T2, LEAP/LEHR/HE, ^{131}I, ^{99m}Tc, by Siemens
2015 Lee *et al* (2015a)	PC	Inveon, LSO, ^{123}I, ^{125}I, by Siemens
2015 Spirou *et al* (2015)	C	ECAM, NaI(Tl), ^{99m}Tc, by Siemens
2017 Georgiou *et al* (2017)	PC	γ-eye, CsI(Na), ^{99m}Tc, ^{111}In, ^{177}Lu, by Bioemtech
2017 Costa *et al* (2017)	C	Symbia T2, MEAP, ^{177}Lu, by Siemens
2018 Taherparvar and Sadremomtaz (2018)	PC	prototype, CsI(Na), ^{99m}Tc
2019 Sadremomtaz and Telikani (2019)	PC	HiReSPECT, LEHR, CsI(Na), ^{99m}Tc, by PNP

Simulation of this full size PET scanner was performed. As illustrated in figure 5, a cubic shape was used to minimize dead zones and to simplify the manufacturing process. The CaLIPSO is composed of 4 sectors of 5 × 6 elementary modules. The acquisition FOV are 354 mm (axial) and 307 mm (radial). TMBi is encapsulated within a transparent sapphire window coupled to the MCP-PMT with optical gel. The read-out ionization pad structure is also integrated. The GATE digital detection model used dedicated parameterized modules to simulate the detector response for the ionization and light signal readout. These semi-analytic models were calibrated using detector prototypes. The first estimation of the non-paralyzable dead time was 3.5 μs, corresponding to mean drift time and the shaping time for electronics readout. Estimated spatial resolution of reconstructed images was 1.1 mm in the complete scanner FOV and sensitivity was 17 kcps/MBq.

J-PET long axial FOV PET with plastic scintillators. J-PET is a PET system based on plastic scintillators allowing for a cost-effective total body solution (Moskal *et al* 2019a, 2018, Moskal and Stepień 2020,

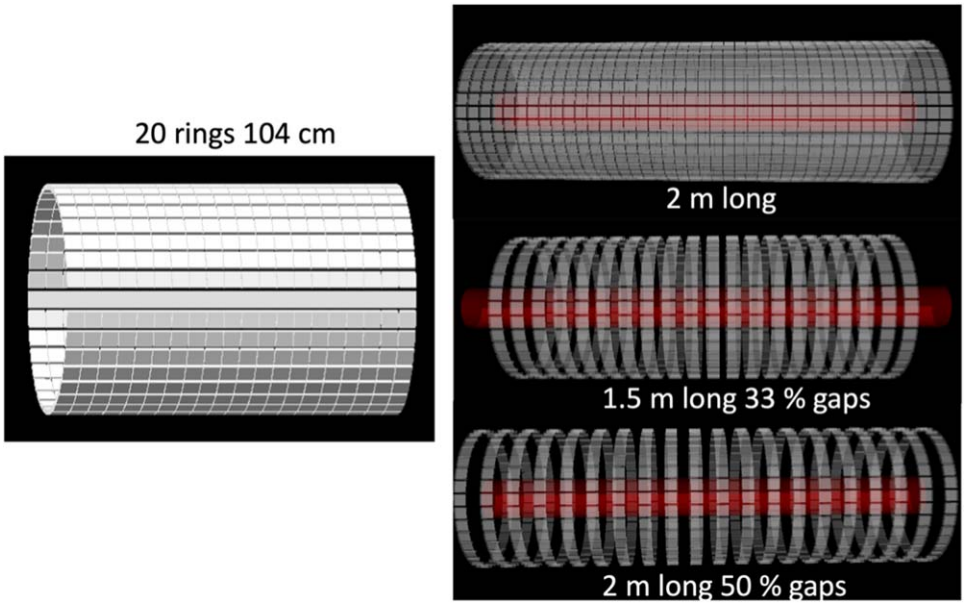

Figure 3. (Left) A long axial FOV scanner of 20 rings (104 cm axial length) based on monolithic scintillator blocks. (right) Long axial FOV systems of 2 m with full coverage, 1.5 m with 33% gaps and a 2 m long system with 50% gaps.

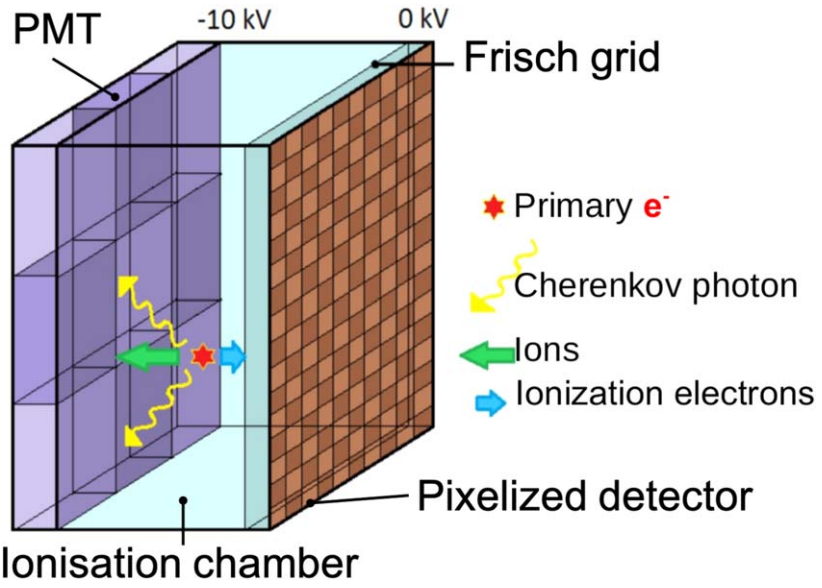

Figure 4. Illustration of unit detector module based on the ionization chamber filled with trimethyl bismuth (TMBi).

Vandenberghe *et al* 2020). The J-PET prototype scanner with a long axial FOV built of axially arranged plastic scintillator strips was simulated in GATE (Kowalski *et al* 2018). Three diameters of the scanner (75, 85 and 95 cm), three lengths (20, 50 and 100 cm) and two thicknesses T (4 and 7 mm) of scintillators were simulated for both single- and double-layer geometries. Spatial resolution was simulated for three readout solutions: (1) vacuum PMT, (2) SiPM matrices and (3) SiPM readout with an additional layer of wavelength shifting (WLS) strips. The WLS were arranged perpendicularly to the scintillator strips, allowing for the determination of the photon interaction point along the tomograph axis, based on the distribution of amplitudes of light signals in WLS strips. The spatial resolution, sensitivity, scatter fraction and NECR were estimated according to the NEMA-NU-2 protocol, as a function of the length of the tomograph, the number of detection layers, the diameter of the tomographic chamber and for various types of applied readout. For the single-layer geometry with a diameter of 85 cm, a strip length of 100 cm, a cross-section of 4 mm $\times$ 20 mm and SiPM with an additional layer of WLS strips as the readout, the spatial resolution FWHM in the center of the scanner was estimated to 3 mm (radial, tangential) and 6 mm (axial). For the analogous double-layer geometry with the same

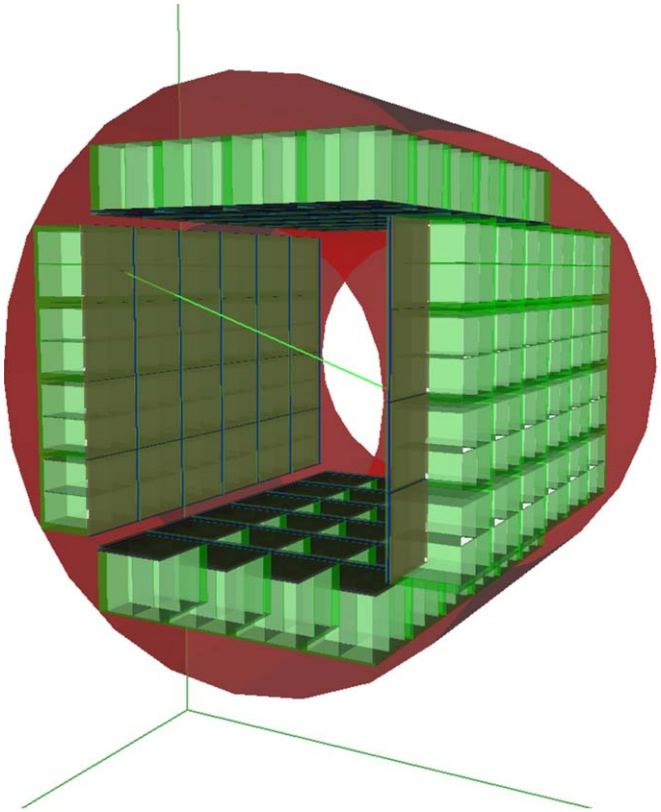

Figure 5. Design of the CaLIPSO PET scanner dedicated for high resolution brain imaging.

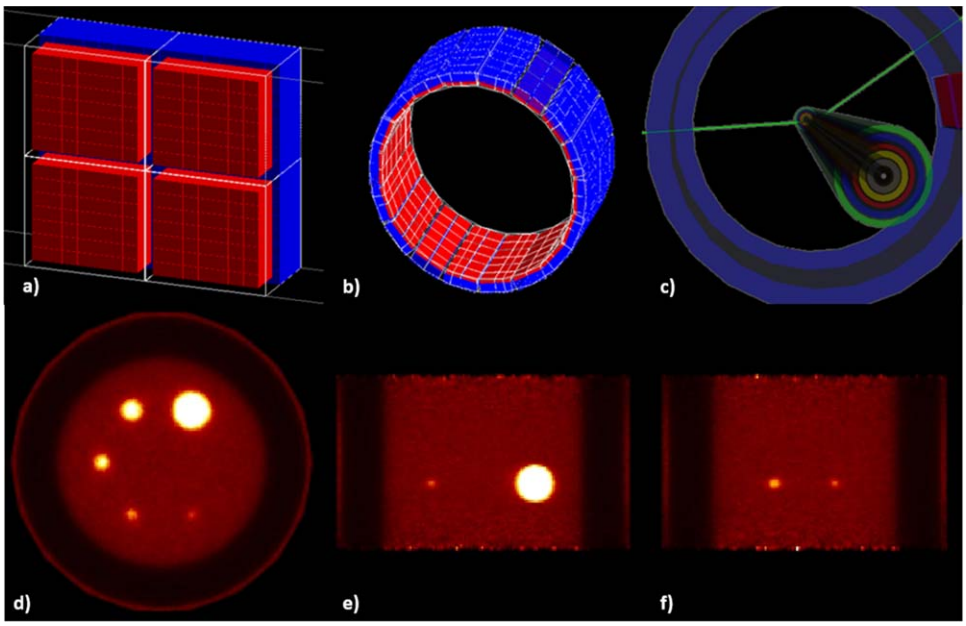

Figure 6. Presentation of the (a) modeled module of the system (1st layer in red and 2nd layer in blue), (b) scheme of the full TRIMAGE scanner in GATE, reprinted from Del Guerra *et al* 2018, Copyright (2018), with permission from Elsevier. Copyright. © European Psychiatric Association 2018. (c) view of the simulated phantom geometry for the sensitivity measurements (the several layers of the sleeves are presented with different colors) and (d)–(f) transversal, coronal and sagittal slices of the 10 iterations of the simulated IQ phantom.

readout, diameter and scintillator length, with a strip cross-section of 7 mm × 20 mm, a NECR peak of 300 kcps was reached at 40 kBq/c.c. activity concentration, the scatter fraction was estimated to be about 35% and the sensitivity at the center amounts to 14.9 cps/kBq.

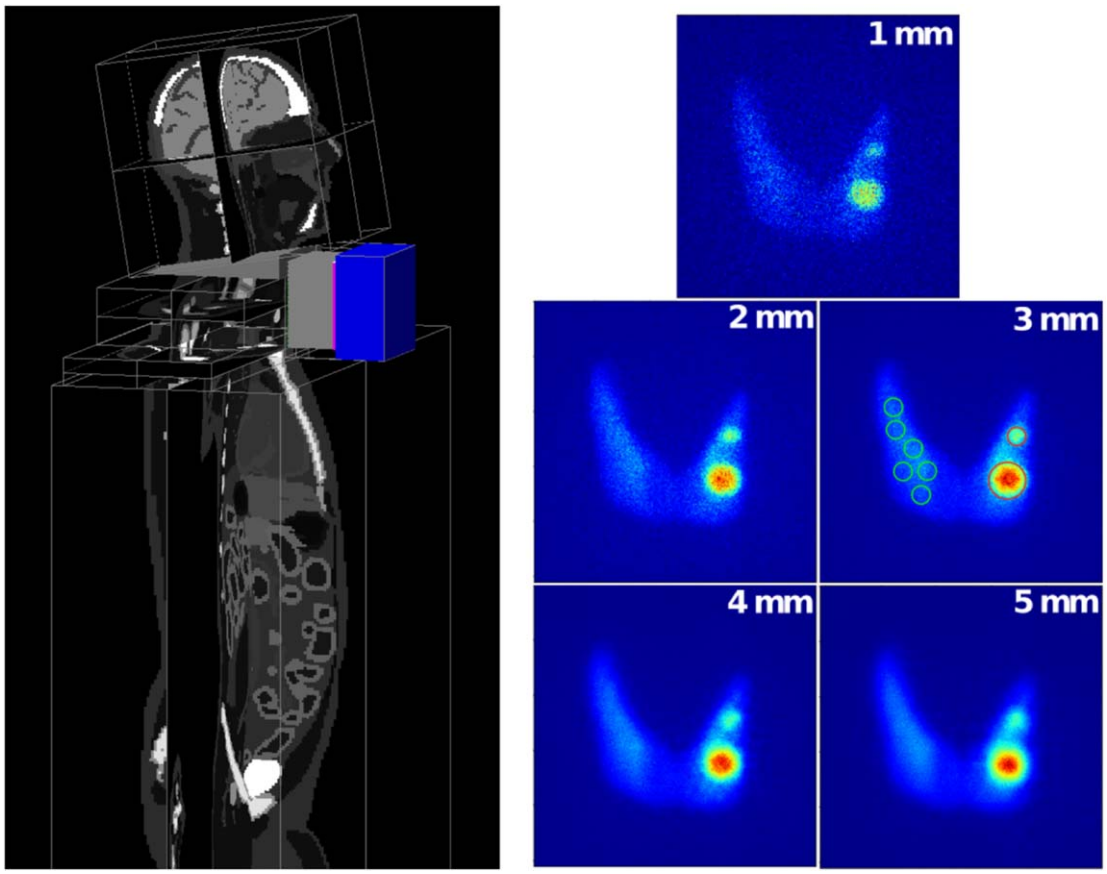

Figure 7. Simulation set-up used for the choice of the collimator. Left—the complete camera and a 3D XCAT voxelized phantom. Right—images of the thyroid with two hot nodules (0.6 and 1.2 cm diameter) simulated for five collimators. Given values are the collimator spatial resolutions. Example of ROIs defined around the nodules and on the background are shown on the 3 mm SR collimator image.

TRIMAGE: trimodality imaging for schizophrenia. A novel dedicated trimodality (PET/MR/EEG) imaging prototype for schizophrenia was developed within the TRIMAGE project. The brainPET insert was modeled and extensively evaluated with GATE. In Del Guerra *et al* (2018), several geometrical phantoms were implemented, covering realistic imaging situations. The simulated PET model was evaluated for its performance (spatial resolution, sensitivity and count rate) according to the NEMA standards. Figure 6 depicts the modeled scanner alongside with the NU 2-2001 sensitivity phantom (Teräs *et al* 2007) and the PRESTO reconstructions of the NU2-1994 Image Quality (IQ) phantom. Spatial resolution varied between 2.34 mm and 3.66 mm (FWHM) axially moving radially 10–100 mm from the center of the FOV. The simulated coincidence efficiency (i.e. the sensitivity) for a point source positioned at the center of the FOV was 61 cps/kBq. To assess the count rates, a solid, cylindrical phantom made of polyethylene (density 0.96 $\pm$ 0.1 g cm^{-3}) with dimensions of 70 mm in length and 25 mm in diameter was used. The phantom was placed at the center of the axial and transaxial FOV of the modeled scanner. A cylindrical hole of 3.2 mm diameter was drilled parallel to the central axis of the cylinder, at a radial distance of 10 mm from the center. The line source insert was a clear polyethylene plastic tube 60 mm in length, filled with 5 to 11 kBq ml^{-1} of ^{18}F and threaded through the hole in the phantom for 1000 s measurement time. The NECR showed a peak above 1.8 Mcps at 250 MBq.

The γ-eye SPECT camera. In Ricci *et al* (2019), the γ-eye, a small FOV preclinical scintigraphic camera was extensively validated. The γ-eye is produced by BIOEMTECH and is suitable for *in vivo* molecular imaging of radiolabeled biomolecules providing a screening tool for dynamic pharmacokinetics studies (Georgiou *et al* 2017). The γ-eye detector was simulated with GATE and evaluated for its spatial resolution and sensitivity properties comparing experimental and simulated data. All of the appropriate electromagnetic and physical processes were included, while no cuts or variance reduction techniques (VRT) were applied. A maximum difference, equal to $\approx$16%, on spatial resolution observed, at 7.5 mm distance (5.85 mm experimental value versus 4.9 mm simulation value). In the case of sensitivity, the difference recorded in zero mm source-to-collimator distance (57 cps/MBq versus 63 cps/MBq) was $\approx$10.5%. For all the other distances the difference in sensitivity was lower and very close to the mean value of 56 cps/MBq.

THIDOS compact mobile γ-camera for absorbed radiation dose control in molecular radiotherapy. The THIDOS project aims to the optimization of the individualized patient dosimetry in radioiodine therapy of thyroid diseases by the development of new instrumental and methodological approaches to strengthen the control of the absorbed dose by reducing the uncertainties associated to dose calculation. In that framework we are developing a high-resolution compact and mobile planar γ-camera with a 10×10 cm^2 FOV for use at the patient bedside. The goal is to improve the individual quantitative assessment of the distribution and biokinetics of radioiodine in target regions and organs-at-risk before and after treatment administration. In Trigila (2019), the design of the high-energy parallel-hole tungsten collimator was optimized using GATE and an XCAT 3D voxelized phantom with realistic background and thyroid gland ^{131}I distributions in order to improve quantification of small targets (nodules or tumor remnants) as shown in figure 7. The camera was fully modeled and a specific study was carried out on the energy and spatial distributions of scattered and penetration events inside the collimator. The best compromise in terms of contrast and signal-to-noise ratio on nodules of various sizes was achieved with a 5.5 cm thick collimator with 1.1 mm hexagonal holes and 0.75 mm thick septa, which allows to minimize the partial volume effect, while reducing both scattered and penetration events (effective septal penetration less than 7.5%). The expected spatial resolution (2 mm FWHM) and efficiency (1.24×10^{-5}) for a ^{131}I source set a 5 cm from the collimator were found to be in good agreement with the experimental results.

MACACO Compton Camera prototype. In Etxebeste *et al* (2020), the first version of MACACO (Medical Applications CompAct COmpton camera) prototype (Muñoz *et al* 2017) built at IFIC-Valencia, was employed for the validation of GATE CCMod against experimental data. This prototype is based on multiple (2–3) layers of $LaBr_3$ monolithic crystals coupled to SiPMs. A system configuration of two layers separated by 50 mm was considered. The crystal sizes were $27.2 \times 26.8 \times 5$ mm^3 and $32 \times 36 \times 10$ mm^3 for the first and second layer respectively both coupled to SiPM arrays with active area pixels of 3×3 mm^2. The first layer was based on four Hamamatsu MPPC S11830-3340MF monolithic arrays whereas the second one was based on an older version S11064-050P(X1) with larger gaps between the pixels. Passive material of the prototype (boards, holders, etc) was also included in the simulations. The performance of the system was characterized and compared to simulated data in terms of energy spectra, efficiency, angular resolution and back-projection image onto the plane of the source with good agreement. Hence, the angular resolution measure for 1275 keV incident photons was $13.4° \pm 0.2°$ (simulation) versus $13.5° \pm 0.2°$ (experimental). Relative detection efficiency was slightly overestimated 2.6×10^{-3} (simulated) versus 1.9×10^{-3} (experimental) and consistent results within a 3-sigma interval were obtained for energy spectra except for low energies where small differences were observed. These discrepancies were partially caused by the approximations made in the simulation of the experimental discriminator threshold at SiPM pixel level in the digitization process which allow us to avoid the generation and transport of optical photons.

Other applications in interventional nuclear medicine. As nuclear medicine techniques make rapid advancement in surgery and in interventional radiology, we briefly summarize the current uses of GATE in support of these applications. They include simulations of tomography units and 1D and 2D detectors with the goal either to enhance the extracted diagnostic information or to maximize the therapeutic effect of the procedures. Following is a list of GATE uses in radio-guided surgery, in trans-arterial radioembolization and in real-time PET/CT guided biopsies.

In radio-guided surgery, GATE is used to simulate gamma and beta detection probes (Spadola *et al* 2016) and optimize the imaging process. Vetter *et al* (2015) used GATE to evaluate the limits of accuracy of an analytical approach to register a previous 3D SPECT image to the readings from an optically tracked hand-held 1D gamma probe an approach known as freehand (fh) SPECT. Since in fh-SPECT the detector positions are arbitrary and the system matrix is not defined, Hartl *et al* (2015) used GATE to simulate a LUT of detector readings at a predefined grid of probe positions around a ^{99m}Tc source in order to obtain the contribution of each source voxel to the detector readings. A LUT created with GATE was used for the fh-SPECT part of a novel hybrid probe combining fh-SPECT with fh-fluorescence (van Oosterom *et al* 2020). The authors used a measured LUT for the optical probe. They commented, that while fluorescence simulations are possible with GATE, the optical LUT computation would be challenging since the opto-nuclear probe is not in direct tissue contact which leads to a dynamic ratio of air and skin contributions (van Oosterom *et al* 2020). In an another development, the design of a PET-like limited angle tomography system for intraoperative radio-guided imaging was explored using GATE by Sajedi *et al* (2019).

After trans-arterial radioembolization of liver tumors with ^{90}Y microspheres, verification of the correct delivery of the microspheres and voxel-based dosimetry can be achieved by performing ^{90}Y SPECT or ^{90}Y PET scans (Bastiaannet *et al* 2018). Since ^{90}Y is a pure β-emitter, the bremsstrahlung radiation used for SPECT imposes the use of broad energy windows which contain large amounts of scattered radiation. In that case, a different Monte Carlo code (SIMIND) was used to optimize the collimators and the energy window for ^{90}Y SPECT (Roshan *et al* 2016). ^{90}Y PET is challenging due to the very low positron yield (3.186×10^{-5}) and Strydhorst *et al* performed a detailed analysis of the sources of quantification error in ^{90}Y PET by separating true coincidences from random and true events caused by the ^{176}Lu LSO crystal activity and by bremsstrahlung

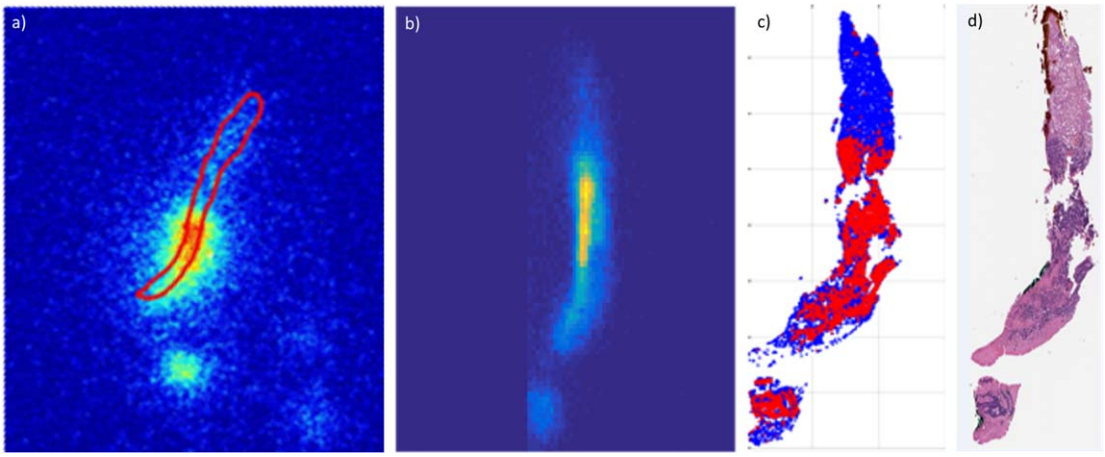

Figure 8. Measured (a) and simulated (b) autoradiography (ARG) images of a liver specimen obtained from ^{18}F-FDG PET/CT guided biopsy. The simulation was performed by building within GATE a 3D voxelized source model of the distribution of tumor cells in the biopsy specimen by registering and stacking 2D slices ((c), only one slice shown) in which the location of tumor cells (red) was obtained by a machine learning tool (TMARKER Schüffler *et al* 2013) applied to the 58 pathology sections (d) into which the specimen was sectioned (Seiter *et al* 2018). The images are not to scale and the uptake in normal liver cells (blue in (c)) was set to zero for this simulation (b). Among the other factors causing a difference between the measured and simulated ARG images are deformation of the specimen during processing and inaccuracies in registration between the sections.

radiation in phantom simulations with GATE (Strydhorst *et al* 2016b). The point-spread function of a cone beam SPECT collimator and the projections of a NEMA phantom model for SPECT parallel hole, cone beam and multifocal collimators were simulated with GATE to validate the performance of the Utrecht Monte Carlo system iterative SPECT reconstruction package for fast pre-radioembolization imaging with ^{99m}Tc macroaggregated albumin (99mTc-MAA) (Dietze *et al* 2018). GATE was also used for investigating various dosimetry aspects of radioembolization (Papadimitroulas *et al* 2012, Mountris *et al* 2014, Roncali *et al* 2020).

The specimens from real-time PET/CT guided biopsies are radioactive, allowing measurement of the amount and the distribution of the PET tracer contained in them by radioactivity measurements. This concept has been explored to show that autoradiography (ARG) images of the specimens are quantifiable and can aid evaluating adequacy of the specimens for diagnosis and for genomic profiling as well as investigating the specificity of beta emitting radiopharmaceuticals with high resolution (Fanchon *et al* 2015, Fanchon 2016, Maybody *et al* 2016, Kirov *et al* 2018). GATE simulations of the positron transport through liver specimens and gelatin-based specimen models which were used for calibrating the ARG detectors were performed to obtain a gel-to-liver correction factor (Fanchon 2016, Kirov *et al* 2018). Further, an ARG image of the tumor cells in a colorectal cancer liver specimen was simulated from the distribution of tumor cells as established in the pathology slices into which the specimen was sectioned (Seiter *et al* 2018), see figure 8.

4. Methodological developments within GATE

In addition to developments dedicated to improve detector modeling, which are detailed in section 2, we briefly review in the following sections recent features added in GATE that help to design emission tomography simulation but are not specific to imaging.

4.1. Towards simpler analysis via Python

Historically, Geant4 and High Energy Physics community are linked to the ROOT CERN framework (Brun and Rademakers 1997) that allows to efficiently manage and analyze physics data. Since the beginning, GATE also allows to write ROOT files, e.g. detector events or phase space, or use them as input, e.g. use phase space file as a source of particles. Python has become the tool of choice for data analysis with modules such as NumPy (Harris *et al* 2020) or Matplotlib (Hunter 2007). Since version 9.0, GATE now includes additional options to read/write data in NPY file format (Harris *et al* 2020) that can be processed with Python. Also, ROOT files can be processed in Python with the uproot module (Pivarski 2020). Details about the NPY file format can be found in the GATE user guide[25] and examples of Python analysis are available on the GateContrib repository[26].

[25] https://opengate.readthedocs.io
[26] https://github.com/OpenGATE/GateContrib

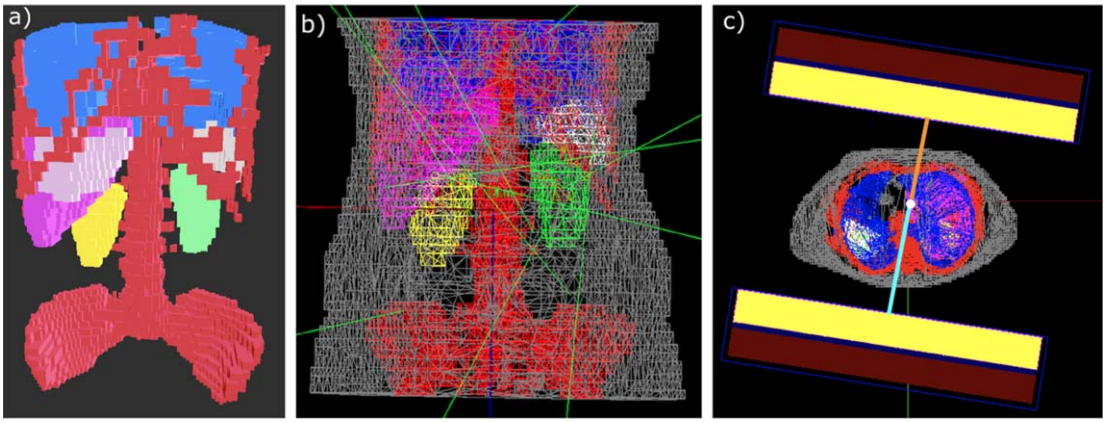

Figure 9. a) Patient mesh model with all segmented volumes of interest: bones (red), lungs (blue), liver (pink), spleen (white) and left and right kidney (green and yellow). (b) Snapshot of patient model with the remainder of the body (gray) from GATE. Few green lines represent photons emissions. (c) Visualization of the auto-contouring gamma camera motion in GATE. Unequal distances of each detector from the center of rotation (in orange and blue respectively) shows that the camera moves in a non-circular orbit.

Finally, the GATE community recently started a new repository, called GateTools[27], that gather Python functions that can be useful for simulation setup and analysis. As example, it contains tools to convert or resize images in various file formats, to convert DICOM RT structures, to manage phase-space files or analyze dose map, with DVH (Dose Volume Histogram) or gamma-index for example. All tools are available as Python function and as command-line independent scripts. At the time of writing, there are more than twenty different tools. The installation is very easy thanks to conventional Python `pip install`. Like GATE itself, the code is open-source and community driven. It should evolve in the future thanks to users' contributions.

4.2. Variance reduction techniques

Several VRTs were developed in GATE. Among those useful for emission tomography, we can describe the following: for particles with relatively large mean free path lengths comparatively to voxels size, Woodcock tracking (Rehfeld *et al* 2009) using fictitious interactions can be used to speed up tracking; for SPECT simulation, angular response function (ARF) (Song and Segars 2005, Descourt *et al* 2010, Sarrut *et al* 2018) replaces the detector response by an analytical (or neural network) model providing probabilities of detection in all energy channels; ARF can be combined with fixed forced detection that forces the detection of a photon in each detector pixel weighted by the probability of emission (or scattering) and transmission to this pixel (Cajgfinger *et al* 2018). The acceleration of all those approaches can reach one order of magnitude, although it depends on many parameters and on the simulation configurations.

4.3. Positronium source

Positronium is a metastable electron–positron bound state, which is formed approximately up to 40% of the cases in a patient's body before the annihilation. It appears in two quantum modes: *ortho-* and *para-positronium*, which have different physical properties, in particular the ortho-positronium lives three orders of magnitude longer than para-positronium, around: 142 ns versus 0.125 ns, respectively. In the tissue, ortho-positronium mean lifetime strongly depends on the size of intramolecular voids (free volumes between atoms), whereas its formation probability depends on the voids concentration (Moskal and Stepień 2020). In a patient's body the formation probability and the mean lifetime are in function of the bio-fluids and bio-active molecules concentration (Moskal *et al* 2019b). As it was shown in Moskal and Stepień (2020), one can reach the mean lifetime precision of about 20 ps. To measure the positronium lifetime, one needs to use non-pure isotopes emitting prompt gammas.

A set of helper classes was added in GATE for the simulations of the positronium decays. Positronium mean lifetime tomography is one of the examples of a novel PET multiphoton imaging technique proposed recently (Moskal *et al* 2019a). The available positronium decay models are: para-positronium two-photon decay, ortho-positronium three-photon decay and the mixed model decay where users can adjust a relative frequency of two possible positronium decays. The implemented model of ortho-positronium decay products angular distribution is described in Kamińska *et al* (2016). All the model parameters are configurable by user with a simple GATE macro. In addition, an emission of prompt gamma with a predefined emission energy can be

[27] https://github.com/OpenGATE/GateTools

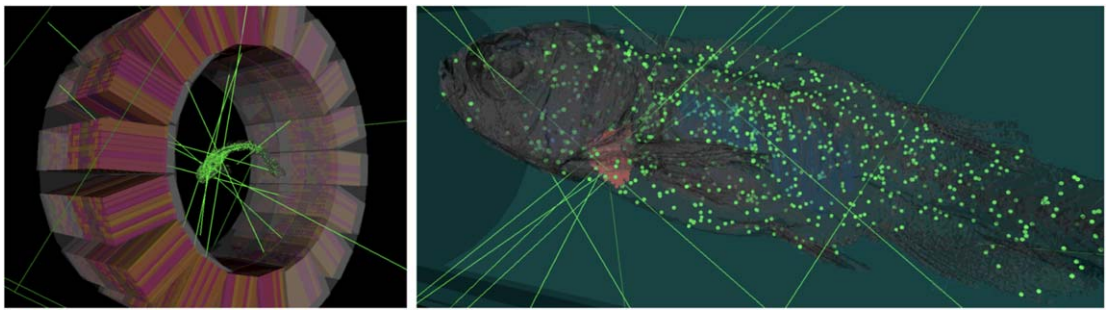

Figure 10. 3D rendering of a custom PET scanner and the MERMAID zebrafish phantom in GATE. Left: full view. Right: zoom to the phantom, placed into a water tube. Here the gray structure represents the tessellated zebrafish volume, and the green and red dots correspond to emission locations for the entire zebrafish and the heart, respectively. The green lines indicate several representative photon trajectories.

added. Photon polarization settings are also supported at the macro level. This source enables advanced PET imaging applications such as oxygen sensing for tumor hypoxia (Shibuya *et al* 2020).

4.4. STL geometry

Thanks to the Geant4 `G4TessellatedSolid` class, tessellated mesh geometries composed of triangle primitives are now available in GATE. Users can import STL (stereolithography) files containing the coordinates of vertices and faces of the meshed surface, and GATE generates the corresponding volume in the geometry. One application of this new kind of geometry has been the modeling of the body contouring limited to cubic shapes allows the gamma camera head to move as close as possible to the phantom/patient model thereby preventing their collision in the GATE environment (Kayal *et al* 2020a, 2020b). Meshes for each segmented volume of interest from the phantom/patient model were generated individually using Python scripts and imported in GATE where individual volumes could be assigned with their respective materials from CT (Kayal *et al* 2021, 2020c). Figure 9 displays the patient mesh model with the auto-contouring gamma camera motion. Total counts in modeled phantom SPECT images obtained with circular and body contouring gamma camera motion with same acquisition parameters revealed a relative difference of around 2.5% and 12% for ^{177}Lu and ^{131}I respectively thereby emphasizing the importance of modeling auto-contouring SPECT gamma camera motion (with the use of STL volumes) especially for radionuclides with high septal penetration (for e.g. ^{131}I). There could be potential activity underestimation caused by the use of circular motion acquisition thereby impacting the absorbed dose in the dosimetry chain.

STL geometries moreover allow for an easy description of complex phantoms, as an alternative to voxelized phantoms. For instance, a STL-based model of a zebrafish was created from ex-vivo high-resolution micro-CT scans (Zvolský *et al* 2019a). This phantom has been designed for the MERMAID project, which is aimed to small-fish PET imaging (Zvolský *et al* 2019b). Figure 10 displays 3D renderings of a PET scanner design and the zebrafish phantom including exemplary photon emissions. Separate STL files were used for different structures (e.g. bones, heart, swim bladder, gills, etc). These meshes were used as both attenuation and emission phantom. As GATE does not support the distribution of activity within a mesh, Geant4 volumes enclosing the tessellated volumes of interest were created. The activity is distributed within the volume by an acceptance-rejection method. Then, GATE confines the emission of radiation to the respective volume with the *confine* method of its General Particle Source. It should be noted that the acceptance-rejection method can significantly slow down the simulation when the surrounding volumes are much larger than the organs or structures of interest to which the activity should be confined. Care should be thus put in selecting the appropriate size and position of the enclosing volumes.

4.5. Link to third-party reconstruction software

Output from PET, SPECT or Compton camera simulation, either as list mode data or projections images can then be used as input for reconstruction software (Gillam and Rafecas 2016). Among others, we can cite the following software used to reconstruct 3D images from GATE simulations. STIR (Software for Tomographic Image Reconstruction) (Thielemans *et al* 2012, Khateri *et al* 2019, Kang *et al* 2018) was among the first to propose dedicated modules allowing to reconstruction GATE simulated data, both for PET and SPECT, with MLEM and OSEM methods. More recently, the CASToR project (Merlin *et al* 2018) (Customizable and Advanced Software for Tomographic Reconstruction) also proposed various reconstruction algorithms for PET and SPECT, with dedicated tools to use GATE generated data. For SPECT images, the QSPECT software (Loudos *et al* 2010, 2014, Spirou *et al* 2015) was also employed, in particular to investigate the effect of

attenuation correction. Recently in Robert *et al* (2019), the Reconstruction Toolkit (RTK) (Rit *et al* 2014) was used to provide 4D whole body SPECT reconstruction using image-based breathing signal extraction (Robert *et al*). The PRESTO toolkit (PET Reconstruction Software Toolkit) (Scheins and Herzog 2008, Scheins *et al* 2011, 2015) can also be used with GATE output, such as in Xu *et al* (2019). Finally, several Compton Camera reconstruction approaches have been used with GATE data, such as in Muñoz *et al* (2018), Kohlhase *et al* (2020) (MLEM or Origin Ensemble) or in Feng *et al* (2020), Maxim (2019) (with conical Radon transform modeling).

4.6. Artificial intelligence integration

There are several potential interactions between artificial intelligence, deep learning in particular, and Monte Carlo simulations. Within the context of medical imaging, these synergies can be classified in two categories. First, Monte Carlo simulations can produce highly accurate imaging device and patient training datasets for neural networks applied to various signal and image processing tasks. At the detector level, multiple works have been carried out to better determine DOI and/or events positioning within pixelated and continuous monolithic scintillators by using trained neural networks (Oliver *et al* 2013, Conde *et al* 2016, Pedemonte *et al* 2017, Berg and Cherry 2018, Müller *et al* 2018, 2019, Iborra *et al* 2019, Yang 2019, Zatcepin *et al* 2020). Training data may be obtained from experimental data acquired with a specific setup or from simulation such as in Yang (2019). In the case of image processing, one can identify tasks specific to the reconstruction and/or the post-processing phase. For example, GATE simulations have been used to provide the input to a U-NET in sinogram space for the derivation of scatter contributions during PET imaging (Visvikis 2020). Deep learning-based scatter correction has been favorably compared with state-of-the art single scatter simulation approaches, independently of the imaging device or anatomical location (tested on lung or pelvis). Similarly, Monte Carlo simulation can generate raw sinograms to training deep-learning networks for PET attenuation correction using MR images (Lee 2020), or for direct deep learning-based image reconstruction in PET imaging (Reader *et al* 2020). In terms of image processing, images generated with GATE have been used as part of the training dataset for a functional tumor volume segmentation challenge. Deep learning-based segmentation approaches trained using this dataset showed improved performance compared to state-of-the-art methods (Hatt *et al* 2018).

Second, deep learning approaches can be applied to improve Monte Carlo simulation performance, mostly computational efficiency. One example is the simulation-trained neural networks to model detector response. In Sarrut *et al* (2018), the authors determined the Angular Response Function (ARF) of a SPECT collimator-detector system with simulation output. The resulting net modeled the probability that a photon is detected, using variance reduction to speed up the simulation. Recently, the concept of generative adversarial networks (GAN) (Goodfellow *et al* 2014) that allow modeling of multidimensional data distributions was proposed to learn a phase space (Sarrut *et al* 2019, 2021) generated by Monte Carlo simulation. Once trained, the generator neural network of the GAN can be used as a very compact source of particles. Similarly, GANs or other more recent variants such as Wasserstein GAN or Deep Convolutional GAN can be applied to generate realistic anthropomorphic models from a few examples of Monte Carlo simulated images with sufficient variability (necessary for training).

Since version 9.0, GATE can be linked to the PyTorch library (Paszke *et al* 2019) and methods to interact with the C++ version of this library have been integrated. Trained neural networks can be loaded and used during particle tracking. This integration opens the door to multiple extensions. Indeed, Monte Carlo can generate data ultimately used to train a net or feed the input layer of a net in order to improve the simulation. Note also that deep learning integration is not limited to emission tomography simulation and can be used for dose estimation (Lee *et al* 2019, Götz *et al* 2019, Nguyen *et al* 2019, Liu *et al* 2019), denoising dose from Monte Carlo simulation both for photon (Peng *et al* 2019, Fornander 2019, Neph *et al* 2019) or proton (Ricardo Asensi Madrigal 2018, Javaid *et al* 2019), scatter modeling (Lalonde *et al* 2020, van der Heyden *et al* 2020), etc. Those studies are still in early stages and further work is needed to better understand the advantages and limitations of mixing deep learning with Monte Carlo approaches. It is a promising field and GATE is ready for it.

5. Conclusion

This article presents an overview of the current status of GATE for emission tomography imaging system simulation, including a large list of systems that have been simulated and, at least partially, validated against experimental data. Recent developments have been described as well and give insight on future improvements in GATE. This comprehensive summary aims at providing an evaluation of the current capabilities and limitations of GATE for imaging systems simulation.

The GATE software has some limitations, partly rooted in the general nature of the Monte Carlo approach, domain-specific problems, and code complexity. First, simulations are generally considered slow, in particular, compared to analytical or semi-analytical methods. Attempts have been made to provide GPU-based

acceleration within GATE (Bert *et al* 2012, 2013) with acceleration factors from 20 to 400 depending on the simulation type. However, GPU integration in GATE was discontinued due to difficulty to support generic enough graphic card types. Part of this work has been ported to the GGEMS Monte Carlo code (Garcia *et al* 2016). One common alternative solution is to apply parallelization techniques by using multiple CPUs (Camarasu-Pop *et al* 2010). Users need, however, to pay attention to the time management in the simulation when splitting into parallel jobs, e.g. dead-time or coincidences sorting. Typically, when splitting a PET simulation into several jobs, each job should keep the same activity rate and the whole simulation should be split according to the total simulated acquisition time. Moreover, true coincidences estimation relies on the particle's ID (identification number) provided by the Geant4 kernel in order to ensure the gamma came from the same events. With parallel independent jobs, each job manage his own set of ID. Events ID from one job cannot be mixed with the ones of another job. Tools are provided to adequately split simulations and to merge job's files such as the events IDs are modified and can be compared.

Computation time also limits the use of optical tracking to the simulation of single or pairs of detectors, due to the need for tracking multiple interactions for each optical photon and the high volume of data recorded. As optical Monte Carlo simulation in radiation detectors is increasingly used to study TOF detectors and prompt photons, the complexity of the simulations expands and so do the requirements in terms of computational power. The latest developments in emission tomography are likely to utilize more and more optical tracking capabilities, making this shortcoming a high priority. Another difficulty lies in the need to precisely know the material and geometrical information of all elements in an imaging system which is often private information that can only be obtained through NDA, preventing publicly share complete imaging models. Another limitation of GATE is that the code source is rather old, more than 15 years, and acknowledges the contributions of numerous volunteers (more than 70 on the current repository that only keeps track of all authors since 2015). Hence, the size and the diversity of the C++ code, more than 350 000 lines of code, makes it relatively hard to maintain. Currently, an effort has been made to modernize the code and adapt a set of engineering techniques e.g. unit tests and continuous integration to improve the code quality. The GATE code typically quickly follows the Geant4 evolutions, thanks to the high responsiveness and support of the Geant4 community. Geant4 toolkit is at the core of simulation in almost every High Energy Physics experiment at CERN (Albrecht *et al* 2019) and will evolve over the next decade towards various improvements, such as the vectorization technique.

GATE is also used for dosimetry purposes, from optimizing the dose of radiation-based imaging to evaluating absorbed dose distribution during radiation therapy for cancer treatment, in external beam photon and particle therapy, and in internal radionuclide therapy (Jan *et al* 2011, Sarrut *et al* 2014, Grevillot *et al* 2020, Roncali *et al* 2020). For example, GATE is one of major contributors to the OpenDose collaboration that aims at providing the community with free resources for Nuclear Medicine dosimetry (Chauvin *et al* 2020)[28]. Indeed, the possibility to perform in the same framework imaging and dosimetry studies is important, such as in hadrontherapy monitoring (Jan *et al* 2012, Gueth *et al* 2013, Huisman *et al* 2016, Hilaire *et al* 2016) or in the assessment of uncertainties associated with clinical molecular radiotherapy dosimetry (Garcia *et al* 2015)[29].

Numerous collaborations with the major manufacturers in this field (Philips, GE, Siemens, Spectrum Dynamics, etc) show that GATE is used not only in academia but also in industry. It might be difficult to make predictions about future GATE development directions because it is largely guided by users' projects and emerging needs. However, we can mention an ongoing trend such as Python binding, which allows performing GATE data analysis using Python scripts, providing access to a large ecosystem of libraries and tools. Moreover, the integration of PyTorch is just at the beginning and may open the doors to developments exploiting Artificial Intelligence methods.

The range of PET and SPECT imaging biomarkers is rapidly expanding for both diagnostic and nuclear theranostic applications (Czernin *et al* 2019), and fast timing has now become a key issue for further improving TOF-PET image contrast and reducing radioactive doses injected to the patients (Lecoq *et al* 2020). Along the incentive proposed by the 10 ps challenge[30], crossing the ambitious 10 ps FWHM CTR frontier which would allow to image a volume virtually without tomographic inversion will necessitate effective, rapid and versatile optical simulation tools to model fast scintillation and prompt photons. In this context, new imaging systems and concepts are being developed to become more quantitative and more cost-effective (Surti *et al* 2020). The OpenGATE collaboration[31] is committed to follow this evolution providing an open-source simulation toolkit dedicated both to research and industry applications in the field of medical imaging, and perhaps numerous other domains utilizing ionizing radiation imaging, such as prompt gamma ray imaging for particle range

[28] https://opendose.org
[29] http://dositest.org
[30] https://the10ps-challenge.org
[31] https://opengatecollaboration.org

monitoring in hadrontherapy, x-ray photon counting and neutron imaging for homeland security, or Compton imaging for nuclear decommissioning and nuclear waste management.

Acknowledgments

The Opengate collaboration would like to warmly thanks the Geant4 collaboration for their great support and fruitful discussions.

This work was performed within the framework of the SIRIC LYriCAN Grant INCa-INSERM-DGOS-12563, the LABEX PRIMES (ANR-11-LABX-0063) of Université de Lyon, within the program 'Investissements d'Avenir' (ANR- 11-IDEX-0007) operated by the ANR, and the POPEYE ERA PerMed 2019 project (ANR-19-PERM-0007-04). Optical modeling developments were supported by NIH grants R03 EB020097 and R01 EB027130. STL related work was performed and supported by the MRTDosimetry project[32] which is funded by EMPIR program co-financed by the Participating States and from the European Unions Horizon 2020 research and innovation program. The patient images used were obtained as a part of IAEA Coordinated Research Project (CRP) on 'Dosimetry in Radiopharmaceutical therapy for personalized patient treatment' (E2.30.05). It has also received support by the ENEN+ project that has received funding from the Euratom research and training Work program 2016-2017-1 #75576. The simulations of this work have been performed on the HPC centre CALMIP. The THIDOS project was partially funded by the IN2P3. The section on applications in interventional nuclear medicine was funded in part by the Marie-Josée and Henry R. Kravis Center for Molecular Oncology at MSK and by the National Cancer Institute Cancer Center Core Grant N. P30-CA008748.

ORCID iDs

David Sarrut https://orcid.org/0000-0002-4854-4141
Maxime Chauvin https://orcid.org/0000-0003-1999-2161
Konstantinos Chatzipapas https://orcid.org/0000-0003-4006-9304
Mathieu Dupont https://orcid.org/0000-0001-5228-5608
Ane Etxebeste https://orcid.org/0000-0001-6280-9268
Assen S Kirov https://orcid.org/0000-0001-6521-3582
Paweł Kowalski https://orcid.org/0000-0002-3545-3865
Joey Labour https://orcid.org/0000-0002-5602-3178
Christian Morel https://orcid.org/0000-0001-5359-6504
Panagiotis Papadimitroulas https://orcid.org/0000-0002-5981-6149
Mariele Stockhoff https://orcid.org/0000-0003-2835-5498
Carlotta Trigila https://orcid.org/0000-0002-0414-9369
Karl Ziemons https://orcid.org/0000-0001-5744-7290
Milan Zvolský https://orcid.org/0000-0003-4300-0871
Emilie Roncali https://orcid.org/0000-0002-2439-1064

References

Abi Akl M, Bouhali O, Toufique Y, Karp J S and Vandenberghe S 2019 Monte Carlo sensitivity study of a long axial FOV PET scanner with patient adaptive rings *2019 IEEE Nucl. Science Symp. and Med. Imaging Conf. (NSS/MIC)* **2019** 1–3

Aklan B, Jakoby B W, Watson C C, Braun H, Ritt P and Quick H H 2015 GATE Monte Carlo simulations for variations of an integrated PET/MR hybrid imaging system based on the bograph mMR model *Phys. Med. Biol.* **60** 4731–52

Albrecht J *et al* 2019 A roadmap for HEP software and computing R&D for the 2020s *Comput. Softw. Big Sci.* **3** 7

Allison J *et al* 2016 Recent developments in GEANT4 *Nucl. Instrum. Methods Phys. Res.* A **835** 186–225

Ariño-Estrada G, Roncali E, Selfridge A R, Du J, Glodo J, Shah K S and Cherry S R 2020 Study of Čerenkov light emission in the semiconductors TlBr and TlCl for TOF-PET *IEEE Trans. Rad. Plasma Med. Sci.* 1

Assie K, Gardin I, Vera P and Buvat I 2004 Validation of gate Monte Carlo simulations for indium 111 imaging *IEEE Symp. Conf. Rec. Nuclear Science* **2004** 4023–7

Assié K *et al* 2004 Monte Carlo simulation in PET and SPECT instrumentation using GATE *Nucl. Instrum. Methods Phys. Res.* A **527** 180–9

Autret D, Bitar A, Ferrer L, Lisbona A and Bardiès M 2005 Monte Carlo modeling of gamma cameras for I-131 imaging in targeted radiotherapy *Cancer Biother. Radiopharmaceuticals* **20** 77–84

Bastiaannet R, Cheenu Kappadath S, Braat A J A T, Lam M G E H and Hugo W A M 2018 The physics of radioembolization *EJNMMI Phys.* **5** 22

Bataille F, Comtat C, Jan S and Trebossen R 2004 Monte Carlo simulation for the ECAT HRRT using GATE *IEEE Symp. Conf. Rec. Nuclear Science* **4** 2570–4

[32] https://mrtdosimetry-empir.eu

Berg E and Cherry S R 2018 Using convolutional neural networks to estimate time-of-flight from PET detector waveforms *Phys. Med. Biol.* **63** 02LT01

Bert J, Perez-Ponce H, Bitar Z E, Jan S, Boursier Y, Vintache D, Bonissent A, Morel C, Brasse D and Visvikis D 2013 Geant4-based Monte Carlo simulations on GPU for medical applications *Phys. Med. Biol.* **58** 5593–611

Bert J *et al* 2012 Hybrid GATE: A GPU/CPU implementation for imaging and therapy applications *2012 IEEE Nucl. Science Symp. and Med. Imaging Conf. Record (NSS/MIC)* **2012** 2247–50

Boisson F, Bekaert V, El Bitar Z, Wurtz J, Steibel J and Brasse D 2011 Characterization of a rotating slat collimator system dedicated to small animal imaging *Phys. Med. Biol.* **56** 1471–85

Brun R and F Rademakers 1997 ROOT—an object oriented data analysis framework *Nucl. Instrum. Methods Phys. Res.* A **389** 81–6

Brunner S E and D R Schaart 2017 BGO as a hybrid scintillator/Cherenkov radiator for cost-effective time-of-flight PET *Phys. Med. Biol.* **62** 4421–39

Bruyndonckx P, Lemaître C, Schaart D, Maas M, (jan) van der Laan D J, Krieguer M, Devroede O and Tavernier S 2007 Towards a continuous crystal APD-based PET detector design *Nucl. Instrum. Methods Phys. Res.* A **571** 182–6

Buvat I and Lazaro D 2006 Monte Carlo simulations in emission tomography and GATE: An overview *Nucl. Instrum. Methods Phys. Res.* **569** 323–9

Cabello J and Ziegler S I 2018 Advances in PET/MR instrumentation and image reconstruction *Br. J. Radiol.* **91** 20160363

Cajgfinger T, Rit S, Létang J M, Halty A and Sarrut D 2018 Fixed forced detection for fast SPECT Monte-Carlo simulation *Phys. Med. Biol.* **63** 055011

Camarasu-Pop S, Glatard T, Mościcki J T, Benoit-Cattin H and Sarrut D 2010 Dynamic partitioning of GATE Monte-Carlo simulations on EGEE *J. Grid Comput.* **8** 241–59

Canot C, Alokhina M, Abbon P, Bard J P, Tauzin G, Yvon D and Sharyy V 2017 Development of the fast and efficient gamma detector using Cherenkov light for TOF-PET *J. Instrum.* **12** C12029

Carlier T, Moisan M, Ferrer L, Kraeber-Bodere F, Barbet J and Bardies M 2008 Validation of a GATE model of the Siemens Symbia system for 99mTc, 111In and 131I acquisitions *J. Nucl. Med.* **49** 405P (https://jnm.snmjournals.org/content/49/supplement_1/405P.1)

Cates J W, Gundacker S, Auffray E, Lecoq P and Levin C S 2018 Improved single photon time resolution for analog SiPMs with front end readout that reduces influence of electronic noise *Phys. Med. Biol.* **63** 185022

Chauvin M *et al* 2020 OpenDose: Open access resources for nuclear medicine dosimetry *J. Nucl. Med.* **119** 1514–9

Cherry S R, Sorenson J A and Phelps M E 2012 *Physics in Nuclear Medicine* ed W B Saunders (Philadelphia: Elsevier) (https://www.elsevier.com/books/physics-in-nuclear-medicine/cherry/978-1-4160-5198-5)

Chung Y H, Choi Y, Cho G, Choe Y S, Lee K-H and Kim B-T 2005 Optimization of dual Layer phoswich detector consisting of LSO and LuYAP for small animal PET *IEEE Trans. Nucl. Sci.* **52** 217–21

Conde P *et al* 2016 Determination of the interaction position of gamma photons in monolithic scintillators using neural network fitting *IEEE Trans. Nucl. Sci.* **63** 30–6

Conti M and Bendriem B 2019 The new opportunities for high time resolution clinical TOF PET *Clin. Transl.l Imaging* **7** 139–47

Costa G C A, Bonifácio D A B, Sarrut D, Cajgfinger T and Bardiès M 2017 Optimization of GATE simulations for whole-body planar scintigraphic acquisitions using the XCAT male phantom with 177Lu-DOTATATE biokinetics in a Siemens Symbia T2 *Phys. Med.* **42** 292–7

Czernin J, Sonni I, Razmaria A and Calais J 2019 The future of nuclear medicine as an independent specialty *J. Nucl. Med.* **60** 3S–12S

Decuyper M, Stockhoff M and Van Holen R 2019 Deep learning for positioning of gamma interactions in monolithic PET detectors *2019 IEEE Nucl. Sci. Symp. and Medi.Imaging Conf. (NSS/MIC), Abstracts*

Decuyper M, Stockhoff M and Van Holen R 2021 Artificial neural networks for positioning of gamma interactions in monolithic PET detectors *Phys. Med. Biol.* **66** 075001

Degenhardt C, Prescher G, Frach T, Thon A, de Gruyter R, Schmitz A and Ballizany R 2009 The digital silicon photomultiplier—anovel sensor for the detection of scintillation light *2009 IEEE Nuc. Sci. Symp. Conf. .Record (NSS/MIC)* **2009** 2383–6

Del Guerra A *et al* 2018 TRIMAGE: a dedicated trimodality (PET/MR/EEG) imaging tool for schizophrenia *Eur. Psychiatry* **50** 7–20

Descourt P, Carlier T, Du Y, Song X, Buvat I, Frey E C, Bardies M, Tsui B M W and Visvikis D 2010 Implementation of angular response function modeling in SPECT simulations with GATE *Phys. Med. Biol.* **55** N253–66

Dietze M M A, van der Velden S, Lam M G E H, Viergever M A and de Jong H W A M 2018 Fast quantitative reconstruction with focusing collimators for liver SPECT *EJNMMI Phys.* **5** 28

Mehadji B 2020 Modélisation Monte Carlo d'une caméra Compton basée sur l'utilisation de détecteurs à scintillation sensibles à la position couplés à des SiPM PhD Thesis Aix-Marseille Université *J. Instrum.*

Emami A, Ghafarian P, Ghadiri H, Geramifar P and Ay M R 2020 Validation and evaluation of a GATE model for MAMMI PET scanner *Iran. J. Nucl. Med.* **28** 33–8 (https://irjnm.tums.ac.ir/article_35815.html)

Etxebeste A, Barrio J, Muñoz E, Oliver J F, Solaz C and Llosá G 2016 3D position determination in monolithic crystals coupled to SiPMs for PET *Phys. Med. Biol.* **61** 3914–34

Etxebeste A, Dauvergne D, Fontana M, Létang J M, Llosá G, Munoz E, Oliver J F, Testa É and Sarrut D 2020 CCMod: a GATE module for Compton camera imaging simulation *Phys. Med. Biol.* **65** 055004

Everett D B, Fleming J S, Todd R W and Nightingale J M 1977 Gamma-radiation imaging system based on the Compton effect *Proc. Inst. Electr. Eng.* **124** 995–1000

Fanchon L 2016 Autoradiographie Quantitative d'échantillons Prélevés Par Biopsie Guidée Par TEP/TDM: Méthode et Applications Cliniques *Thèse de doctorat en Biologie Santé,* Brest (http://www.theses.fr/2016BRES0018)

Fanchon L M *et al* 2015 Feasibility of *in situ*, high-resolution correlation of tracer uptake with histopathology by quantitative autoradiography of biopsy specimens obtained under 18F-FDG PET/CT guidance *J. Nucl. Med.* **56** 538–44

Feng Y, Etxebeste A, Sarrut D, Létang J M and Maxim V 2020 3-D Reconstruction benchmark of a compton camera against a parallel-hole gamma camera on ideal data *IEEE Trans. Radiat. Plasma Med. Sci.* **4** 479–88

Fornander H 2019 Denoising Monte Carlo Dose Calculations Using a Deep Neural Network *PhD Thesis,* KTH Royal Institute Of Technology School of Electrical Engineering and Computer Science (https://www.diva-portal.org/smash/get/diva2:1366439/FULLTEXT01.pdf)

Frach T, Prescher G, Degenhardt C, de Gruyter R, Schmitz A and Ballizany R 2009 The digital silicon photomultiplier—principle of operation and intrinsic detector performance *2009 IEEE Nuclear Science Symp. Conf. Record (NSS/MIC)* pp 1959–65

Garcia M-P, Bert J, Benoit D, Bardiès M and Visvikis D 2016 Accelerated GPU based SPECT Monte Carlo simulations *Phys. Med. Biol.* **61** 4001–18

Garcia M-P, Villoing D, McKay E, Ferrer L, Cremonesi M, Botta F, Ferrari M and Bardiès M 2015 TestDose: a nuclear medicine software based on Monte Carlo modeling for generating gamma camera acquisitions and dosimetry *Med. Phys.* **42** 6885–94
Georgiou M, Fysikopoulos E, Mikropoulos K, Fragogeorgi E and Loudos G 2017 Characterization of "γ-Eye": a low-cost benchtop mouse-sized gamma camera for dynamic and static imaging studies *Mol. Imaging Biol.* **19** 398–407
Geramifar P, Ay M R, Shamsaie Zafarghandi M, Loudos G and Rahmim A 2009 Performance comparison of four commercial GE discovery PET/CT scanners: a monte carlo study using GATE *Iran. J. Nucl. Med.* **17** 26–33 (https://irjnm.tums.ac.ir/article_533.html)
Geramifar P, Ay M R, Shamsaie Zafarghandi M, Sarkar S, Loudos G and Rahmim A 2011 Investigation of time-of-flight benefits in an LYSO-based PET/CT scanner: a Monte Carlo study using GATE *Nucl. Instrum. Methods Phys. Res.* A **641** 121–7
Gillam J E and Rafecas M 2016 Monte-Carlo simulations and image reconstruction for novel imaging scenarios in emission tomography *Nucl. Instrum. Methods Phys. Res.* A **809** 76–88
Gonias P *et al* 2007 Validation of a GATE model for the simulation of the Siemens biograph^{TM} 6 PET scanner *Nucl. Instrum. Methods Phys. Res.* A **571** 263–6
Goodfellow I, Pouget-Abadie J, Mirza M, Xu B, Warde-Farley D, Ozair S, Courville A and Bengio Y 2014 Generative adversarial nets *Advances in Neural Information Processing Systems* (*NIPS'14*) vol 2 (Montreal, Canada: MIT) pp 2672–80
Götz T I, Schmidkonz C, Chen S, Al-Baddai S, Kuwert T and Lang E W 2020 A deep learning approach to radiation dose estimation *Phys. Med. Biol.* **65** 035007
Grevillot L *et al* 2020 GATE-RTion: a GATE/Geant4 release for clinical applications in scanned ion beam therapy *Med. Phys.* **47** 3675–81
Groiselle C J, Kudrolli H A and Glick S J 2004 Monte-Carlo simulation of the photodetection systems prototype PET scanner using GATE: a validation study *IEEE Symp. Conf. Record Nuclear Science* **2004** 3130–2
Gueth P, Dauvergne D, Freud N, Létang J M, Ray C, Testa E and Sarrut D 2013 Machine learning-based patient specific prompt-gamma dose monitoring in proton therapy *Phys. Med. Biol.* **58** 4563–77
Harris C R *et al* 2020 Array programming with NumPy *Nature* **585** 357–62
Hartl A, Shakir D I, Lasser T, Ziegler S I and Navab N 2015 Detection models for freehand SPECT reconstruction *Phys. Med. Biol.* **60** 1031–46
Hatt M *et al* 2018 The first MICCAI challenge on PET tumor segmentation *Med. Image Anal.* **44** 177–95
Hilaire E, Sarrut D, Peyrin F and Maxim V 2016 Proton therapy monitoring by Compton imaging: influence of the large energy spectrum of the prompt-γ radiation *Phys. Med. Biol.* **61** 3127
Huisman B F B, Létang J M, Testa É and Sarrut D 2016 Accelerated prompt gamma estimation for clinical proton therapy simulations *Phys. Med. Biol.* **61** 7725
Hunter J D 2007 Matplotlib: a 2D graphics environment *Comput. Sci. Eng.* **9** 90–5
Iborra A, González A J, González-Montoro A, Bousse A and Visvikis D 2019 Ensemble of neural networks for 3D position estimation in monolithic PET detectors *Phys. Med. Biol.* **64** 195010
Jan S, Comtat C, Strul D, Santin G and Trebossen R 2005 Monte Carlo simulation for the ECAT EXACT HR+ system using GATE *IEEE Trans. Nucl. Sci.* **52** 627–33
Jan S, Frisson T and Sarrut D 2012 GATE simulation of 12C hadrontherapy treatment combined with a PET imaging system for dose monitoring: a feasibility study *IEEE Trans. Nucl. Sci.* **60** 423–9
Jan S *et al* 2004 GATE: a simulation toolkit for PET and SPECT *Phys. Med. Biol.* **49** 4543–61
Jan S *et al* 2011 GATE V6: a major enhancement of the GATE simulation platform enabling modelling of CT and radiotherapy *Phys. Med. Biol.* **56** 881–901
Javaid U, Souris K, Dasnoy D, Huang S and Lee J A 2019 Mitigating inherent noise in Monte Carlo dose distributions using dilated U-net *Med. Phys.* **46** 5790–8
Kamińska D *et al* 2016 A feasibility study of ortho-positronium decays measurement with the J-PET scanner based on plastic scintillators *Eur. Phys. J.* C **76** 445
Kang H G, Tashima H, Hong S J and Yamaya T 2018 Optimization of a high resolution small animal SPECT system using GATE and STIR software *2018 IEEE Nuc. Sci. Symp. and Medical Imaging Conf. Proc.(NSS/MIC)* **2018** 1–3
Karakatsanis N *et al* 2006 Comparative evaluation of two commercial PET scanners, ECAT EXACT HR+ and Biograph 2, using GATE *Nucl. Instrum. Methods Phys. Res.* A **569** 368–72
Kayal G, Chauvin M, Gil A V, Clayton N, Ferrer L, Moalosi T, Knoll P, Struelens L and Bardies M 2021 Generation of clinical 177Lu SPECT/CT images based on Monte Carlo simulation with GATE *Phys. Med.*
Kayal G, Chauvin M, Mora-Ramirez E, Clayton N, Vergara Gil A, Tran-Gia J, Lassmann M, Struelens L and Bardies M 2020a Modeling SPECT auto-contouring acquisition for 177Lu & 131I Molecular Radiotherapy using new developments in Geant4/GATE submitted
Kayal G, Chauvin M, Mora-Ramirez E, Struelens L and Bardies M 2020b Implementation of SPECT auto-contouring detector motion in GATE Monte Carlo simulation for 177Lu and 131I molecular radiotherapy (MRT) dosimetry *Eur J Nucl Med Mol Imaging* **47** 1–753
Kayal G, Chauvin M, Vergara Gil A, Clayton N, Struelens L and Bardies M 2020c Generation of realistic SPECT/CT images for 177Lu dosimetry in molecular radiotherapy (MRT) based on Monte Carlo simulation with GATE *European Association of Nuclear Medicine (EANM) Annual Congress* 47, pp 1–753
Khateri P, Fischer J, Lustermann W, Tsoumpas C and Dissertori G 2019 Implementation of cylindrical PET scanners with block detector geometry in STIR *EJNMMI Phys.* **6** 15
Kirov A S *et al* 2018 Technical Note: Scintillation well counters and particle counting digital autoradiography devices can be used to detect activities associated with genomic profiling adequacy of biopsy specimens obtained after a low activity 18 F-FDG injection *Med. Phys.* **45** 2179–85
Kochebina O, Jan S, Stute S, Sharyy V, Verrecchia P, Mancardi X and Yvon D 2019 Performance estimation for the high resolution CaLIPSO brain PET scanner: a simulation study *IEEE Trans. Radiat. Plasma Med. Sci.* **3** 363–70
Kohlhase N, Wegener T, Schaar M, Bolke A, Etxebeste A, Sarrut D and Rafecas M 2020 Capability of MLEM and OE to detect range shifts with a compton camera in particle therapy *IEEE Trans. Radiat. Plasma Med. Sci.* **4** 233–42
Kowalski P *et al* 2018 Estimating the NEMA characteristics of the J-PET tomograph using the GATE package *Phys. Med. Biol.* **63** 165008
Kwon S I, Gola A, Ferri A, Piemonte C and Cherry S R 2016 Bismuth germanate coupled to near ultraviolet silicon photomultipliers for time-of-flight PET *Phys. Med. Biol.* **61** L38–47
Kwon S I, Roncali E, Gola A, Paternoster G, Piemonte C and Cherry S R 2019 Dual-ended readout of bismuth germanate to improve timing resolution in time-of-flight PET *Phys. Med. Biol.* **64** 105007
Lalonde A, Winey B A, Verburg J M, Paganetti H and Sharp G C 2020 Evaluation of CBCT scatter correction using deep convolutional neural networks for head and neck adaptive proton therapy *Phys. Med. Biol.* (https://doi.org/10.1088/1361-6560/ab9fcb)
Lamare F, Turzo A, Bizais Y, Cheze Le Rest C and Visvikis D 2006 Validation of a Monte Carlo simulation of the Philips Allegro/GEMINI PET systems using GATE *Phys. Med. Biol.* **51** 943–62

Lazaro D *et al* 2004 Validation of the GATE Monte Carlo simulation platform for modelling a CsI(Tl) scintillation camera dedicated to small-animal imaging *Phys. Med. Biol.* **49** 271–85
Lecoq P 2012 New approaches to improve timing resolution in scintillators *IEEE Trans. Nucl. Sci.* **59** 2313–8
Lecoq P 2017 Pushing the limits in time-of-flight PET imaging *IEEE Trans. Radiat. Plasma Med. Sci.* **1** 473–85
Lecoq P *et al* 2020 Roadmap toward the 10 ps time-of-flight PET challenge *Phys. Med. Biol.* **65** 21RM01
Lee J S 2020 A review of deep learning-based approaches for attenuation correction in positron emission tomography *IEEE Trans. Radiat. Plasma Med. Sci.* 1
Lee M S, Hwang D, Kim J H and Lee J S 2019 Deep-dose: a voxel dose estimation method using deep convolutional neural network for personalized internal dosimetry *Sci. Rep.* **9** 10308
Lee S, Gregor J, Kennel S J, Osborne D R and Wall J 2015a GATE validation of standard dual energy corrections in small animal SPECT-CT *PLoS One* **10** e0122780
Lee S, Gregor J and Osborne D 2013 Development and validation of a complete GATE model of the siemens inveon trimodal imaging platform *Mol. Imaging* **12** 7290
Lee Y S, Kim J S, Kim K M, Lim S M and Kim H-J 2015b Determination of energy windows for the triple energy window scatter correction method in I-131 on a Siemens SYMBIA gamma camera: a GATE simulation study *J. Instrum.* **10** P01004
Lehner C E, He Z and Zhang F 2004 4/spl pi/ Compton imaging using a 3-D position-sensitive CdZnTe detector via weighted list-mode maximum likelihood *IEEE Trans. Nucl. Sci.* **51** 1618–24
Lenz M 2020 Design and characterisation of an MRI compatible human brain PET insert by means of simulation and experimental studies *PhD Thesis* Bergische Universität Wuppertal
Lewellen T K 2008 Recent developments in PET detector technology *Phys. Med. Biol.* **53** R287–317
Li S, Zhang Q, Vuletic I, Xie Z, Yang K and Ren Q 2017 Monte Carlo simulation of ray-scan 64 PET system and performance evaluation using GATE toolkit *J. Instrum.* **12** T02001
Liu Z, Fan J, Li M, Yan H, Hu Z, Huang P, Tian Y, Miao J and Dai J 2019 A deep learning method for prediction of three-dimensional dose distribution of helical tomotherapy *Med. Phys.* **46** 1972–83
Loudos G K, Papadimitroulas P, Zotos P, Tsougos I and Georgoulias P 2010 Development and evaluation of QSPECT open-source software for the iterative reconstruction of SPECT images *Nucl. Med. Commun.* **31** 558–66
Loudos G K, Papadimitroulas P G and Kagadis G C 2014 Exploitation of realistic computational anthropomorphic phantoms for the optimization of nuclear imaging acquisition and processing protocols *Annual Int. Conf. of the IEEE Eng. in Med. and Biology Society* **2014** 1921–4
Lu L, Zhang H, Bian Z, Ma J, Feng Q and Chen W 2016 Validation of a Monte Carlo simulation of the Inveon PET scanner using GATE *Nucl. Instrum. Methods Phys. Res.* A **828** 170–5
Maier D *et al* 2018 Second generation of portable gamma camera based on Caliste CdTe hybrid technology *Nucl. Instrum. Methods Phys. Res.* A **912** 338–42
Maxim V 2019 Enhancement of Compton camera images reconstructed by inversion of a conical radon transform *Inverse Problems* **35** 014001
Maybody M, Grewal R K, Healey J H, Antonescu C R, Fanchon L, Hwang S, Carrasquillo J A, Kirov A and Farooki A 2016 Ga-68 DOTATOC PET/CT guided Biopsy and cryoablation with autoradiography of biopsy specimen for treatment of tumor-induced osteomalacia *Cardiovascular Interventional Radiol.* **39** 1352–7
McIntosh B, Stout D B and Goertzen A L 2011 Validation of a GATE model of ^{176}Lu intrinsic radioactivity in LSO PET systems *IEEE Trans. Nucl. Sci.* **58** 682–6
Merheb C, Nicol S, Petegnief Y, Talbot J-N and Buvat I 2006 Assessment of the mosaic animal PET system response using list-mode data for validation of GATE Monte Carlo modelling *Nucl. Instrum. Methods Phys. Res.* A **569** 220–4
Merlin T, Stute S, Benoit D, Bert J, Carlier T, Comtat C, Filipovic M, Lamare F and Visvikis D 2018 CASToR: A generic data organization and processing code framework for multi-modal and multi-dimensional tomographic reconstruction *Phys. Med. Biol.* **63** 185005
Michel C, Eriksson L, Rothfuss H, Bendriem B, Lazaro D and Buvat I 2006 Influence of crystal material on the performance of the HiRez 3D PET scanner: A Monte-Carlo study *IEEE Nuclear Science Symp. Conf. Record* **2006** 2528–31
Mihailescu L, Vetter K M, Burks M T, Hull E L and Craig W W 2007 SPEIR: a Ge Compton camera *Nucl. Instrum. Methods Phys. Res.* A **570** 89–100
Mok G S P, Du Y, Wang Y, Frey E C and Tsui B M W 2010 Development and validation of a Monte Carlo simulation tool for multi-pinhole SPECT *Mol. Imaging Biol.* **12** 295–304
Monnier F, Fayad H, Bert J, Schmidt H and Visvikis D 2015 Validation of a simultaneous PET/MR system model for PET simulation using GATE *EJNMMI Phys.* **2** A45
Montémont G, Bohuslav P, Dubosq J, Feret B, Monnet O, Oehling O, Skala L, Stanchina S, Verger L and Werthmann G 2017 NuVISION: a Portable Multimode Gamma Camera based on HiSPECT Imaging Module *2017 IEEE Nuc. Sci. Symp. and Med. Imaging Conf. (NSS/MIC)* **2017** 1–3
Moraes E R, Poon J K, Balakrishnan K, Wang W and Badawi R D 2015 Towards component-based validation of GATE: aspects of the coincidence processor *Phys. Med.* **31** 43–8
Moskal P, Jasińska B, Stepień E and Bass S D 2019b Positronium in medicine and biology *Nat. Rev. Phys.* **1** 527–9
Moskal P and Stepień E 2020 Prospects and clinical perspectives of total-body PET imaging using plastic scintillators *PET Clinics* **15** 439–52
Moskal P *et al* 2018 Feasibility studies of the polarization of photons beyond the optical wavelength regime with the J-PET detector *Eur. Phys. J.* C **78** 970
Moskal P *et al* 2019a Feasibility study of the positronium imaging with the J-PET tomograph *Phys. Med. Biol.* **64** 055017
Mountris K, Autret A, Papadimitroulas P, Loudos G, Visvikis D and Nikiforidis G 2014 Optimization of image-based dosimetry in Y90 radioembolization: a Monte Carlo approach using the GATE simulation toolkit *Phys. Med.: Eur. J. Med. Phys.* **30** e47
Müller F, Schug D, Hallen P, Grahe J and Schulz V 2018 Gradient tree boosting-based positioning method for monolithic scintillator crystals in positron emission tomography *IEEE Trans. Radiat. Plasma Med. Sci.* **2** 411–21
Müller F, Schug D, Hallen P, Grahe J and Schulz V 2019 A novel algorithm for monolithic scintillator crystals in PET based on gradient tree boosting *IEEE Trans. Radiat. Plasma Med. Sci.* **3** 465–74
Muñoz E, Barrio J, Bernabéu J, Etxebeste A, Lacasta C, Llosá G, Ros A, Roser J and Oliver J F 2018 Study and comparison of different sensitivity models for a two-plane Compton camera *Phys. Med. Biol.* **63** 135004
Muñoz E, Barrio J, Etxebeste A, Ortega P G, Lacasta C, Oliver J F, Solaz C and Llosá G 2017 Performance evaluation of MACACO: a multilayer Compton camera *Phys. Med. Biol.* **62** 7321–41

Neph R, Huang Y, Yang Y and Sheng K 2019 DeepMCDose: a deep learning method for efficient monte carlo beamlet dose calculation by predictive denoising in MR-guided radiotherapy *Artificial Intelligence in Radiation Therapy* ed D Nguyen *et al* 11 850 (Cham: Springer International Publishing,) p 137–45

Nguyen D, Jia X, Sher D, Lin M-H, Iqbal Z, Liu H and Jiang S 2019 3D radiotherapy dose prediction on head and neck cancer patients with a hierarchically densely connected U-net deep learning architecture *Phys. Med. Biol.* **64** 065020

Nikolopoulos D, Kottou S, Chatzisavvas N, Argyriou X, Vlamakis E, Yannakopoulos P and Louizi A 2013 A GATE simulation study of the Siemens biograph DUO PET/CT system *Open J. Radiol.* **2013** 56–65

Oliver J F, Fuster-Garcia E, Cabello J, Tortajada S and Rafecas M 2013 Application of artificial neural network for reducing random coincidences in PET *IEEE Trans. Nucl. Sci.* **60** 3399–409

Papadimitroulas P, Loudos G, Nikiforidis G C and Kagadis G C 2012 A dose point kernel database using GATE Monte Carlo simulation toolkit for nuclear medicine applications: comparison with other Monte Carlo codes *Med. Phys.* **39** 5238–47

Park M-J, Park K-S, Lee J-S, Kim Y-K and Lee D-S 2009 Validation of a GATE model for the simulation of a trionix TRIAD SPECT camera *J. Korean Phys. Soc.* **55** 681–7

Paszke A *et al* 2019 PyTorch: an imperative style, high-performance deep learning library *NEURIPS 2019* **32** 8024–35 (https://proceedings.neurips.cc/paper/2019/file/bdbca288fee7f92f2bfa9f7012727740-Paper.pdf)

Pedemonte S, Pierce L and Van Leemput K 2017 A machine learning method for fast and accurate characterization of depth-of-interaction gamma cameras *Phys. Med. Biol.* **62** 8376–401

Peng Z, Shan H, Liu T, Pei X, Zhou J, Wang G and Xu X G 2019 Deep learning for accelerating Monte Carlo radiation transport simulation in intensity-modulated radiation therapy arXiv:(1910.07735) [physics]

Pivarski J *et al* 2020 Scikit-hep/uproot: 3.12.0 *Zenodo* (https://doi.org/10.5281/zenodo.3543691)

Poon J K, Dahlbom M L, Casey M E, Qi J, Cherry S R and Badawi R D 2015 Validation of the SimSET simulation package for modeling the siemens biograph mCT PET scanner *Phys. Med. Biol.* **60** N35–45

Poon J K, Dahlbom M L, Moses W W, Balakrishnan K, Wang W, Cherry S R and Badawi R D 2012 Optimal whole-body PET scanner configurations for different volumes of LSO scintillator: a simulation study *Phys. Med. Biol.* **57** 4077–94

Rannou F R, Kohli V, Prout D L and Chatziioannou A F 2004 Investigation of OPET performance using GATE, a Geant4-based simulation software *IEEE Trans. Nucl. Sci.* **51** 2713–7

Reader A J, Corda G, Mehranian A, da Costa-Luis C, Ellis S and Schnabel J A 2020 Deep learning for PET image reconstruction *IEEE Trans. Radiat. Plasma Med. Sci.* **5** 1–25

Rechka S, Fontaine R, Rafecas M and Lecomte R 2009 Development and validation of a GATE simulation model for the LabPET scanner *IEEE Trans. Nucl. Sci.* **56** 3672–9

Rehfeld N S, Stute S, Apostolakis J, Soret M and Buvat I 2009 Introducing improved voxel navigation and fictitious interaction tracking in GATE for enhanced efficiency *Phys. Med. Biol.* **54** 2163–78

Rey M, Jan S, Vieira J M, Mosset J B, Krieguer M, Comtat C and Morel C 2007 Count rate performance study of the Lausanne ClearPET scanner demonstrator *Nucl. Instrum. Methods Phys. Res.* A **571** 207–10

Ricardo Asensi Madrigal J 2018 Deep learning approach for denoising Monte Carlo Dose distribution in proton therapy *PhD Thesis* Université Catholique de Louvain thesis:14550 (http://hdl.handle.net/2078.1/thesis:14550)

Ricci R, Kostou T, Chatzipapas K, Fysikopoulos E, Loudos G, Montalto L, Scalise L, Rinaldi D and David S 2019 Monte Carlo optical simulations of a small FoV gamma camera. effect of scintillator thicknesses and septa materials *Crystals* **9** 398

Rit S, Vila Oliva M, Brousmiche S, Labarbe R, Sarrut D and Sharp G C 2014 The Reconstruction Toolkit (RTK), an open-source cone-beam CT reconstruction toolkit based on the Insight Toolkit (ITK) *J. Phys.: Conf. Ser.* **489** 012079

Robert A, Rit S, Baudier T, Jomier J and Sarrut D 2019 4D respiration-correlated whole-body SPECT reconstruction *2019 IEEE NSS-MIC* (https://www.eventclass.org/contxt_ieee2019/online-program/session?s=M-13)

Robert C, Montémont G, Rebuffel V, Verger L and Buvat I 2011 Optimization of a parallel hole collimator/CdZnTe gamma-camera architecture for scintimammography *Med. Phys.* **38** 1806–19

Roncali E and Cherry S R 2011 Application of silicon photomultipliers to positron emission tomography *Ann. Biomed. Eng.* **39** 1358–77

Roncali E and Cherry S R 2013 Simulation of light transport in scintillators based on 3D characterization of crystal surfaces *Phys. Med. Biol.* **58** 2185–98

Roncali E, Kwon S I, Jan S, Berg E and Cherry S R 2019 Cerenkov light transport in scintillation crystals explained: realistic simulation with GATE *Biomed. Phys. Eng. Express* **5** 035033

Roncali E, Taebi A, Foster C and Vu C T 2020 Personalized dosimetry for liver cancer Y-90 radioembolization using computational fluid dynamics and Monte Carlo simulation *Ann. Biomed. Eng.* **48** 1499–510

Roshan H R, Mahmoudian B, Gharepapagh E, Azarm A and Pirayesh Islamian J 2016 Collimator and energy window optimization for ^{90}Y bremsstrahlung SPECT imaging: a SIMIND Monte Carlo study *Appl. Radiat. Isot.* **108** 124–8

Sadremomtaz A and Telikani Z 2019 Validation and optimization studies of small animal SPECT using GATE Monte Carlo simulation *Nucl. Instrum. Methods Phys. Res.* A **915** 94–101

Sajedi S, Blackberg L, Fakhri G E, Choi H S and Sabet H 2019 Intraoperative radio-guided imaging system for surgical applications *J. Nucl. Med.* **60** 317

Sakellios N, Rubio J L, Karakatsanis N, Kontaxakis G, Loudos G, Santos A, Nikita K and Majewski S 2006 GATE simulations for small animal SPECT/PET using voxelized phantoms and rotating-head detectors *2006 IEEE Nuclear Science Symp. Conf. Record* **2006** 2000–3

Salvadori J, Labour J, Odille F, Marie P-Y, Badel J-N, Imbert L and Sarrut D 2020 Monte Carlo simulation of digital photon counting PET *EJNMMI Phys.* **7** 23

Santin G, Strul D, Lazaro D, Simon L, Krieguer M, Martins M V, Breton V and Morel C 2003 GATE: a Geant4-based simulation platform for PET and SPECT integrating movement and time management *IEEE Trans. Nucl. Sci.* **50** 1516–21

Sarrut D, Krah N, Badel J N and Létang J M 2018 Learning SPECT detector angular response function with neural network for accelerating Monte-Carlo simulations *Phys. Med. Biol.* **63** 205013

Sarrut D, Krah N and Létang J M 2019 Generative adversarial networks (GAN) for compact beam source modelling in Monte Carlo simulations *Phys. Med. Biol.* **64** 215004

Sarrut D *et al* 2014 A review of the use and potential of the GATE Monte Carlo simulation code for radiation therapy and dosimetry applications *Med. Phys.* **41** 064301

Sarrut D, Etxebeste A, Krah N and Létang JM 2021 Modeling complex particles phase space with GAN for Monte Carlo SPECT simulations: a proof of concept *Phys. Med. Biol.* **66** 055014

Schaart D R, Ziegler S and Zaidi H 2020 Achieving 10 ps coincidence time resolution in TOF-PET is an impossible dream *Med. Phys.* **47** 2721–4

Scheins J J and Herzog H 2008 PET reconstruction software toolkit—PRESTO a novel, universal C++ library for fast, iterative, fully 3D PET image reconstruction using highly compressed, memory-resident system matrices *IEEE Nuclear Science Symp. Conf. Record* **2008** 4147–50

Scheins J J, Herzog H and Shah N J 2011 Fully-3D PET image reconstruction using scanner-independent, adaptive projection data and highly rotation-symmetric voxel assemblies *IEEE Trans. Med. Imaging* **30** 879–92

Scheins J J, Vahedipour K, Pietrzyk U and Shah N J 2015 High performance volume-of-intersection projectors for 3D-PET image reconstruction based on polar symmetries and SIMD vectorisation *Phys. Med. Biol.* **60** 9349–75

Schmidtlein C R, Kirov A S, Nehmeh S A, Erdi Y E, Humm J L, Amols H I, Bidaut L M, Ganin A, Stearns C W, McDaniel D L and Hamacher K A 2006 Validation of GATE Monte Carlo simulations of the GE advance/discovery LS PET scanners *Med. Phys.* **33** 198–208

Schüffler P J, Fuchs T J, Ong C S, Wild P J, Rupp N J and Buhmann J M 2013 TMARKER: a free software toolkit for histopathological cell counting and staining estimation *J. Pathol. Inform.* **4** S2

Seiter D *et al* 2018 Quantity and location of the tumor cells in a biopsy specimen *J. Nucl. Med.* **59** 248 (https://jnm.snmjournals.org/content/59/supplement_1/248)

Sharyy V *et al* 2016 Efficient and fast 511-keV Γ detection through Cherenkov radiation: the CaLIPSO optical detector *J. Instrum.* **11** P11008

Sheikhzadeh P, Sabet H, Ghadiri H, Geramifar P, Mahani H, Ghafarian P and Ay M R 2017 Development and validation of an accurate GATE model for NeuroPET scanner *Physica Med.* **40** 59–65

Shibuya K, Saito H, Nishikido F, Takahashi M and Yamaya T 2020 Oxygen sensing ability of positronium atom for tumor hypoxia imaging *Commun. Phys.* **3** 1–8

Solevi P *et al* 2013 A Monte-Carlo based model of the AX-PET demonstrator and its experimental validation *Phys. Med. Biol.* **58** 5495–510

Somlai-Schweiger I and Ziegler S I 2015 CHERENCUBE: Concept definition and implementation challenges of a Cherenkov-based detector block for PET *Med. Phys.* **42** 1825–35

Song X, Segars W P, Du Y, Tsui B M W and Frey E C 2005 Fast modelling of the collimator–detector response in Monte Carlo simulation of SPECT imaging using the angular response function *Phys. Med. Biol.* **50** 1791–804

Spadola S, Verdier M-A, Pinot L, Esnault C, Dinu N, Charon Y, Duval M-A and Ménard L 2016 Design optimization and performances of an intraoperative positron imaging probe for radioguided cancer surgery *J. Instrum.* **11** P12019

Spirou S V, Papadimitroulas P, Liakou P, Georgoulias P and Loudos G 2015 Investigation of attenuation correction in SPECT using textural features, Monte Carlo simulations, and computational anthropomorphic models *Nucl. Med. Commun.* **36** 952–61

Staelens S, Koole M, Vandenberghe S, D'Asseler Y, Lemahieu I and Van de Walle R 2005 The geometric transfer function for a slat collimator mounted on a strip detector *IEEE Trans. Nucl. Sci.* **52** 708–13

Staelens S, Strul D, Santin G, Vandenberghe S, Koole M, D'Asseler Y, Lemahieu I and Van de Walle R 2003 Monte Carlo simulations of a scintillation camera using GATE: Validation and application modelling *Phys. Med. Biol.* **48** 3021–42

Staelens S, Vunckx K, De Beenhouwer J, Beekman F, D'Asseler Y, Nuyts J and Lemahieu I 2006 GATE simulations for optimization of pinhole imaging *Nucl. Instrum. Methods Phys. Res.* A **569** 359–63

Stockhoff M, Jan S, Dubois A, Cherry S R and Roncali E 2017 Advanced optical simulation of scintillation detectors in GATE V8.0: First implementation of a reflectance model based on measured data *Phys. Med. Biol.* **62** L1–8

Stockhoff M, Van Holen R and Vandenberghe S 2019 Optical simulation study on the spatial resolution of a thick monolithic PET detector *Phys. Med. Biol.* **64** 195003

Strul D, Santin G, Lazaro D, Breton V and Morel C 2003 GATE (geant4 application for tomographic emission): a PET/SPECT general-purpose simulation platform *Nucl. Phys.* B **125** 75–9

Strydhorst J and Buvat I 2016a Redesign of the GATE PET coincidence sorter *Phys. Med. Biol.* **61** N522–31

Strydhorst J, Carlier T, Dieudonné A, Conti M and Buvat I 2016b A gate evaluation of the sources of error in quantitative 90Y PET *Med. Phys.* **43** 5320

Surti S, Guerra A D and Zaidi H 2020 Total-body PET is ready for prime time *Med. Phys.* **48** 3–6

Tabacchini V, Westerwoudt V, Borghi G, Seifert S and Schaart D R 2014 Probabilities of triggering and validation in a digital silicon photomultiplier *J. Instrum.* **9** P06016

Taherparvar P and Sadremomtaz A 2018 Development of GATE Monte Carlo simulation for a CsI pixelated gamma camera dedicated to high resolution animal SPECT *Australas. Phys. Eng. Sci. Med.* **41** 31–9

Teräs M, Tolvanen T, Johansson J J, Williams J J and Knuuti J 2007 Performance of the new generation of whole-body PET/CT scanners: discovery STE and Discovery VCT *Eur. J. Nucl. Med. Mol. Imaging* **34** 1683–92

Thielemans K, Tsoumpas C, Mustafovic S, Beisel T, Aguiar P, Dikaios N and Jacobson M W 2012 STIR: Software for tomographic image reconstruction release 2 *Phys. Med. Biol.* **57** 867–83

Trigila C 2019 Development of a portable gamma imaging system for absorbed radiation dose control in molecular radiotherapy *PhD Thesis* Université Paris-Saclay (https://tel.archives-ouvertes.fr/tel-02475983/document)

Trigila C, Moghe E and Roncali E 2021 Standalone application to generate custom reflectance Look-Up Table for advanced optical Monte Carlo simulation in GATE/Geant4 *Med Phys.* (to appear) (https://doi.org/10.1002/mp.14863)

Trindade A *et al* 2012 Validation of GATE Monte Carlo simulations of the Philips GEMINI TF and TruFlight Select PET/CT scanners based on NEMA NU2 standards *2012 IEEE Nuc. Sci. Symp. and Med. Imaging Conf. Record (NSS/MIC)* **2012** 2546–9

van der Heyden B *et al* 2020 A Monte Carlo based scatter removal method for non-isocentric cone-beam CT acquisitions using a deep convolutional autoencoder *Phys. Med. Biol.* **65** 145002

van der Laan D J, Maas M C, de Jong H W A M, Schaart D R, Bruyndonckx P, Lemaître C and van Eijk C W E 2007 Simulated performance of a small-animal PET scanner based on monolithic scintillation detectors *Nucl. Instrum. Methods Phys. Res.* A **571** 227–30

van Oosterom M N *et al* 2020 Extending the hybrid surgical guidance concept with freehand fluorescence tomography *IEEE Trans. Med. Imaging* **39** 226–35

Vandenberghe S 2006 Three-dimensional positron emission tomography imaging with 124I and 86Y *Nucl. Med. Commun.s* **27** 237–45

Vandenberghe S, Daube-Witherspoon M E, Lewitt R M and Karp J S 2006a Fast reconstruction of 3D time-of-flight PET data by axial rebinning and transverse mashing *Phys. Med. Biol.* **51** 1603–21

Vandenberghe S, Mikhaylova E, Brans B, Defrise M, Lahoutte T, Muylle K, Van Holen R, Schaart D and Karp J 2017 PET20.0: a cost efficient, 2mm spatial resolution Total Body PET with point sensitivity up to 22% and adaptive axial FOV of maximum 2.00m *Eur J Nucl Med Mol Imaging* **44** 119–956

Vandenberghe S, Moskal P and Karp J S 2020 State of the art in total body PET *EJNMMI Phys.* **7** 35

Vandenberghe S, Van Holen R, Staelens S and Lemahieu I 2006b System characteristics of SPECT with a slat collimated strip detector *Phys. Med. Biol.* **51** 391–405

Vandervoort E, Camborde M-L, Jan S and Sossi V 2007 Monte Carlo modelling of singles-mode transmission data for small animal PET scanners *Phys. Med. Biol.* **52** 3169–84

Vetter C, Lasser T, Okur A and Navab N 2015 1D-3D Registration for Intra-Operative Nuclear Imaging in Radio-Guided Surgery *IEEE Trans. Med. Imaging* **34** 608–17

Visvikis D, Lefevre T, Lamare F, Kontaxakis G, Santos A and Darambara D 2006 Monte Carlo based performance assessment of different animal PET architectures using pixellated CZT detectors *Nucl. Instrum. Methods Phys. Res.* A **569** 225–9

Visvikis D, Merlin T, Bousse A, Benoit D, Laurent B, Visvikis D, Merlin T, Bousse A, Benoit D and Laurent B 2020 Deep learning based scatter correction for PET imaging *Eur J Nucl Med Mol Imaging* **47** 1–753

Xu H, Lenz M, Caldeira L, Ma B, Pietrzyk U, Lerche C, Shah N J and Scheins J 2019 Resolution modeling in projection space using a factorized multi-block detector response function for PET image reconstruction *Phys. Med. Biol.* **64** 145012

Yang C C, Seidel J, Wang Y, Lee J S, Pomper M G and Tsui B M W 2007 Validation of GATE Monte Carlo simulation of the performance characteristics of a GE eXplore VISTA small animal PET system *2007 IEEE Nuclear Science Symp. Conf. Record* vol 4, pp 3187–90

Yang T-Y 2019 Machine Learning for High Resolution 3D Positioning of Gamma-Interactions in Monolithic PET Detectors *Master Thesis* Ghent University

Yvon D, Sharyy V, Follin M, Bard J-P, Breton D, Maalmi J, Morel C and Delagnes E 2020 Design study of a scintronic crystal targeting tens of picoseconds time resolution for gamma ray imaging: the ClearMind detector arXiv:2006.14855v1 [physics]

Zagni F, D'Ambrosio D, Spinelli A E, Cicoria G, Fanti S and Marengo M 2013 Accurate modeling of a small animal PET scanner using GATE *Appl. Radiat. Isot.* **75** 105–14

Zatcepin A, Pizzichemi M, Polesel A, Paganoni M, Auffray E, Ziegler S I and Omidvari N 2020 Improving depth-of-interaction resolution in pixellated PET detectors using neural networks *Phys. Med. Biol.* **65** 175017

Zvolský M, Schreiner N, Seeger S, Schaar M, Rakers S and Rafecas M 2019a Digital zebrafish phantom based on micro-CT data for imaging research *IEEE Nuc. Sci. Symp. and Med. Imaging Conf.(NSS/MIC)* **2019** 1–2

Zvolský M, Seeger S, Schaar M, Schmidt C and Rafecas M 2019b MERMAID—a PET prototype for small aquatic animal imaging. *IEEE Nuc. Sci. Symp. and Med. Imaging Conf. (NSS/MIC)* **2019** 1–2